GEOPHYSICS, VOL. 74, NO. 5 (SEPTEMBER-OCTOBER 2009); P. WB33–WB53, 18 FIGS.
10.1190/1.3197862

Effective reflection coefficients for curved interfaces in transversely isotropic media

Milana Ayzenberg[1], Ilya Tsvankin[2], Arkady Aizenberg[3], and Bjørn Ursin[4]

ABSTRACT

Plane-wave reflection coefficients (PWRCs) are routinely used in amplitude-variation-with-offset analysis and for generating boundary data in Kirchhoff modeling. However, the geometrical-seismics approximation based on PWRCs becomes inadequate in describing reflected wavefields at near- and postcritical incidence angles. Also, PWRCs are derived for plane interfaces and break down in the presence of significant reflector curvature. Here, we discuss effective reflection coefficients (ERCs) designed to overcome the limitations of PWRCs for multicomponent data from heterogeneous anisotropic media. We represent the reflected wavefield in the immediate vicinity of a curved interface by a generalized plane-wave decomposition, which approximately reduces to the conventional Weyl-type integral computed for an apparent source location. The ERC then is obtained as the ratio of the reflected and incident wavefields at each point of the interface. To conduct diffraction modeling, we combine ERCs with the tip-wave superposition method (TWSM), extended to elastic media. This methodology is implemented for curved interfaces that separate an isotropic incidence half-space and a transversely isotropic (TI) medium with the symmetry axis orthogonal to the reflector. If the interface is plane, ERCs generally are close to the exact solution, sensitive to the anisotropy parameters and source-receiver geometry. Numerical tests demonstrate that the difference between ERCs and PWRCs for typical TI models can be significant, especially at low frequencies and in the postcritical domain. For curved interfaces, ERCs provide a practical approximate tool to compute the reflected wavefield. We analyze the dependence of ERCs on reflector shape and demonstrate their advantages over PWRCs in 3D diffraction modeling of PP and PS reflection data.

INTRODUCTION

Plane-wave reflection and transmission coefficients provide the basis for ray-theory treatment of seismic wavefields in layered media. In the geometrical-seismics approximation, which represents the leading term of the ray-series expansion, the amplitude of any wave mode is proportional to the product of the reflection/transmission coefficients along the raypath (Brekhovskikh, 1980; Červený, 2001). For example, the well-known geometrical-seismics expression for a wave reflected from the bottom of a homogeneous layer includes the plane-wave reflection coefficient (PWRC) multiplied by the source radiation function and divided by the geometrical-spreading factor.

However, geometrical-seismics approximations become inaccurate for near- and postcritical incidence angles or when the source and/or receiver is close (compared to the predominant wavelength) to the reflector (Brekhovskikh, 1980; Tsvankin, 1995). Deviations from the geometrical-seismics approximation become much more pronounced in the presence of even moderate seismic anisotropy (Tsvankin, 2005). Also, because PWRCs are derived for plane interfaces, they cannot be used for ray-theory modeling in the presence of significant reflector curvature.

The limitations of the geometrical-seismics approximation pose serious problems for dynamic ray tracing and Kirchhoff integral modeling techniques (Frazer and Sen, 1985; Hanyga and Helle, 1995; Ursin and Tygel, 1997, Červený, 2001; Ursin, 2004). In partic-

Manuscript received by the Editor 21 July 2008; revised manuscript received 6 November 2008; published online 28 September 2009.
[1]Formerly Norwegian University of Science and Technology, Department of Petroleum Engineering and Applied Geophysics, Trondheim, Norway; presently StatoilHydro, Trondheim, Norway. E-mail: mayz@statoilhydro.com.
[2]Colorado School of Mines, Center for Wave Phenomena, Golden, Colorado, U.S.A. E-mail: ilya@dix.mines.edu.
[3]Institute of Petroleum Geology and Geophysics SB RAS, Novosibirsk, Russia. E-mail: aizenbergam@ipgg.nsc.ru.
[4]Norwegian University of Science and Technology, Department of Petroleum Engineering and Applied Geophysics, Trondheim, Norway. E-mail: bjorn.ursin@ntnu.no.

ular, the boundary data used in conventional Kirchhoff modeling are obtained by multiplying the amplitude of the incident wave (which generally has a curved wavefront) by the PWRC. This approach produces artificial diffractions on synthetic data because of the discontinuous slope of the PWRC at the critical angle (Kampfmann, 1988; Wenzel et al., 1990; Sen and Frazer, 1991).

Another practically important method based on geometrical-seismics techniques is amplitude-variation-with-offset (AVO) analysis, which operates with PWRCs estimated from surface reflection data. Furthermore, because of the complexity of exact reflection coefficients, PWRCs used in AVO processing often are linearized in the velocity and density contrasts across the reflector. The weak-contrast approximation of PWRCs is given by Shuey (1985) for isotropic media and extended by Thomsen (1993) and Rüger (1997) to transversely isotropic models with a vertical symmetry axis (VTI). The VTI expressions involve an additional linearization in the anisotropy parameters on both sides of the interface, which helps to separate the reflection coefficient into isotropic and anisotropic terms. Rüger (1997, 2002) generalizes the weak-contrast, weak-anisotropy PWRC equations for azimuthally anisotropic models and discusses their application in fracture characterization using wide-azimuth reflection data.

Whereas PWRCs often are defined through the magnitude of the displacement vector, Chapman (1994) introduces reflection coefficients obtained from the ratio of the energy flux for reflected and incident waves. Schleicher et al. (2001) derive linearized approximations of these coefficients for general anisotropic media. They show that application of the energy-normalized coefficients in Kirchhoff modeling produces reciprocal reflected wavefields. Klimeš (2003) provides general expressions for the weak-contrast energy-normalized reflection and transmission coefficients in arbitrary anisotropic media. Stovas and Ursin (2003) extend the energy-normalized reflection coefficients to viscoelastic VTI media.

However, the linearized approximations lose accuracy with increasing incidence angle and break down near the critical ray. To overcome this problem, Downton and Ursenbach (2006) express the reflection coefficient as a function of the averaged incidence and transmission angles and develop an analytic continuation of the linearized PWRC in the postcritical domain. For weak parameter contrasts across the interface, their approximation remains close to the exact PWRC for postcritical angles.

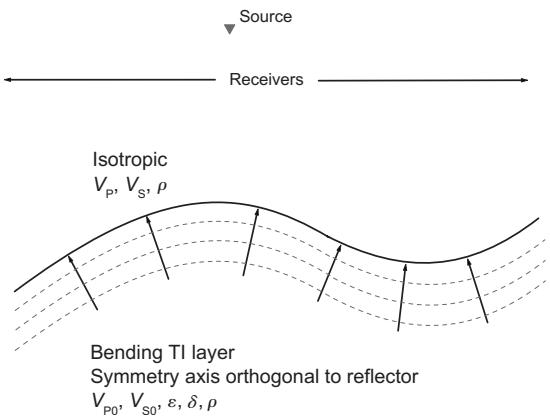

Figure 1. 2D sketch of the model. The isotropic incidence medium is separated from the reflecting TI half-space by a curved interface. The symmetry axis of the TI medium is orthogonal to the reflector. Dashed lines indicate the local orientation of the isotropy plane for the TI layer.

Still, even exact PWRCs used in the geometrical-seismics approximation cannot describe the postcritical reflected wavefield, which includes the interfering head and reflected waves. To make PWRCs suitable for amplitude analysis in the postcritical domain, van der Baan and Smit (2006) propose applying the τ-p transform to wide-angle reflection data. Although the transformed wavefield exhibits a better fit to the corresponding PWRC, the τ-p technique is not strictly valid for laterally heterogeneous media with curved interfaces. Also, seismic data are acquired with finite aperture and often on a sparse spatial grid, which limits the applicability of the τ-p transform.

Brekhovskikh (1980) describes the exact wavefield generated by a point source and reflected from a plane interface through plane-wave decomposition. Červený and Hron (1961) introduce spherical-wave reflection coefficients as the three components of the reflected wavefield at the receiver divided by the geometrical-spreading factor. They show that the new coefficients adequately reproduce the amplitude of the reflected waves and incorporate near-critical and postcritical effects, in particular head waves. However, their methodology is restricted to plane horizontal reflectors and homogeneous media.

Ayzenberg et al. (2007) introduce effective reflection coefficients (ERCs) for reflection of acoustic waves at curved interfaces between inhomogeneous media and demonstrate their advantages in Kirchhoff modeling. Unlike spherical-wave reflection coefficients, ERCs are defined in the vicinity of the reflector. They are designed to generalize PWRCs for wavefields from point sources at curved interfaces and are not limited to small incidence angles and weak parameter contrasts across the reflector. In particular, Kirchhoff modeling with ERCs removes the critical-angle artifacts mentioned above and correctly reproduces the amplitudes of the reflected and head waves.

The goal of this paper is to extend ERCs to curved reflectors in heterogeneous anisotropic models and to implement the new formalism for an interface between isotropic and transversely isotropic (TI) media. We begin the paper by defining ERCs through a generalized plane-wave decomposition similar to the one proposed by Klem-Musatov et al. (2004) for the acoustic problem. Although this solution involves integration over a curved reflecting surface, ERCs can be obtained approximately from Weyl-type integrals computed for apparent spherical waves and locally plane interface segments. Then we conduct numerical tests to evaluate the difference between ERCs and PWRCs for a plane interface and study the dependence of ERCs on the anisotropy parameters, frequency, and local reflector shape. Finally, using the tip-wave superposition method (TWSM), we implement ERCs in 3D elastic diffraction modeling. Tests for curved interfaces of different shapes confirm our algorithm's ability to model reflected wavefields in the presence of multipathing and caustics. Appendices A–F contain the necessary theoretical details.

EFFECTIVE REFLECTION COEFFICIENTS FOR ANISOTROPIC MEDIA

Wavefield representation using surface integrals

We consider the wavefield reflected from a smooth curved interface S that separates two homogeneous half-spaces — isotropic and TI (Figure 1). The point explosive source, located in the isotropic

medium, excites a spherical P-wave. The symmetry axis of the TI half-space is assumed to be locally orthogonal to the reflector. The isotropic medium is described by the P-wave velocity $V_P^{(1)}$, the S-wave velocity $V_S^{(1)}$, and density $\rho^{(1)}$. The TI medium is described by the symmetry-direction velocities of P- and S-waves $V_{P0}^{(2)}$ and $V_{S0}^{(2)}$, density $\rho^{(2)}$, and Thomsen anisotropy parameters ε and δ. Another anisotropy parameter, γ, influences only SH-waves, which are decoupled from P- and SV-waves in our model.

We analyze only the primary P- and SV-wave reflections from the interface and neglect higher-order scattering. Using the representation theorem (Pao and Varatharajulu, 1976; Aki and Richards, 2002), the total reflected wavefield can be described by the surface integral

$$\mathbf{u}(\mathbf{x}) = \int\int_S [\mathbf{u}(\mathbf{x}')\cdot\mathbf{T}(\mathbf{x}',\mathbf{x}) - \mathbf{t}(\mathbf{x}')\cdot\mathbf{G}(\mathbf{x}',\mathbf{x})]\, dS(\mathbf{x}'), \quad (1)$$

where $\mathbf{u}(\mathbf{x}')$ and $\mathbf{t}(\mathbf{x}')$ are the displacement and traction vectors at the interface, and $\mathbf{G}(\mathbf{x}',\mathbf{x})$ and $\mathbf{T}(\mathbf{x}',\mathbf{x})$ are the Green's displacement and traction tensors.

To evaluate integral 1, we use TWSM and split the reflector into small rhombic elements. As discussed in Appendix A, the reflected wavefield can be computed as the sum of tip-wave beams excited by each rhombic element in accordance with Huygens' principle. The PP-wave displacement is obtained in equations A-15 and A-16, which represent an extension of TWSM to elastic media:

$$\mathbf{u}_{PP}(\mathbf{x}) \simeq \sum_j \Delta\mathbf{B}_{PP[j]}(\mathbf{x}), \quad (2)$$

where $\Delta\mathbf{B}_{PP[j]}(\mathbf{x})$ is the vector contribution of the jth surface element, given by

$$\Delta\mathbf{B}_{PP[j]}(\mathbf{x}) = \frac{i\omega}{V_P^{(1)}}\mathbf{l}_{P[j]}(\mathbf{x})\int\int_{\Delta\Pi_{[j]}}\left[\frac{\partial g_P(\mathbf{x}',\mathbf{x})}{\partial n'}d_{1,PP}(\mathbf{x}') - g_P(\mathbf{x}',\mathbf{x})d_{2,PP}(\mathbf{x}')\right]dS'. \quad (3)$$

Here, $\Delta\Pi_{[j]}$ is the area of the surface element, $\mathbf{l}_{P[j]}(\mathbf{x}) = \nabla g_P(\mathbf{x}'_{[j]},\mathbf{x})/|\nabla g_P(\mathbf{x}'_{[j]},\mathbf{x})|$, $g_P(\mathbf{x}',\mathbf{x})$ is the scalar P-wave Green's function, $d_{1,PP}(\mathbf{x}')$ and $d_{2,PP}(\mathbf{x}')$ are the scalar boundary values of the reflected PP-wave at the interface, and $\mathbf{n}'$ is the normal to the reflector directed into the upper medium. Equation A-14 expresses the boundary data $d_{1,PP}$ and $d_{2,PP}$ through the incident wavefield and the PP-wave ERC introduced below.

Each beam $\Delta\mathbf{B}_{PP[j]}$ in equation 3 expresses the contribution of a rhombic element $\Delta\Pi_{[j]}$ to the total reflected wavefield at receiver $\mathbf{x}$. From the computational standpoint, it is important to note that the wavefield $\mathbf{u}_{PP}(\mathbf{x})$ is formed primarily by beams generated inside the Fresnel zone for the specular ray. The contribution of rhombic elements outside the Fresnel zone is relatively small because of destructive interference of the corresponding beams, whose traveltimes are much larger than those of near-specular beams.

Likewise, we show in Appendix A that the reflected PS-wave can be represented as the sum of the tip-wave beams described by equation A-25:

$$\mathbf{u}_{PS}(\mathbf{x}) \simeq \sum_j \Delta\mathbf{B}_{PS[j]}(\mathbf{x}), \quad (4)$$

where $\Delta\mathbf{B}_{PS[j]}(\mathbf{x})$ is the wavefield produced by the jth surface element,

$$\Delta\mathbf{B}_{PS[j]}(\mathbf{x}) = \int\int_{\Delta\Pi_{[j]}}\left[\frac{\partial g_S(\mathbf{x}',\mathbf{x})}{\partial n'}\mathbf{u}_{PS}(\mathbf{x}') - g_S(\mathbf{x}',\mathbf{x}) \times(\nabla'\times\mathbf{u}_{PS}(\mathbf{x}'))\times\mathbf{n}(\mathbf{x}')\right]dS'; \quad (5)$$

$g_S(\mathbf{x}',\mathbf{x})$ is the scalar S-wave Green's function, and $\mathbf{u}_{PS}(\mathbf{x}')$ and $(\nabla'\times\mathbf{u}_{PS}(\mathbf{x}'))\times\mathbf{n}(\mathbf{x}')$ are the vector boundary values, which express the reflected PS-wavefield at the interface.

To evaluate integrals 3 and 5, we use the approximation originally developed by Aizenberg (1992, 1993a, 1993b) for acoustic waves. Here, we generalize the scalar version of his approach for elastic waves. Each vector beam $\Delta\mathbf{B}_{PP[j]}(\mathbf{x})$ or $\Delta\mathbf{B}_{PS[j]}(\mathbf{x})$ is represented by three scalar Cartesian components. Using Stokes' theorem, the integral representation for each component is reduced to the sum of the reflected wave and a contour integral, also known as the Maggi-Rubinowitz contour integral (Baker and Copson, 1953). The contour integral can be approximated by the sum of four edge waves emitted by the edges of the element and eight tip waves emitted by the vertices of the element. Within the boundary layer but outside the vicinity of the edge, the edge waves are described by the Fresnel integral. The tip waves then are described by the generalized Fresnel integral.

Wavefield at the interface in terms of the ERC

In conventional Kirchhoff modeling, it is assumed that the reflected wavefield $\mathbf{u}_{PQ}(\mathbf{x}')$ (subscript Q stands for P or S) at the interface can be approximately written as

$$\mathbf{u}_{PQ}(\mathbf{x}') \simeq R_{PQ}(\theta(\mathbf{x}'))\,[\mathbf{u}_P^{inc}(\mathbf{x}')\cdot\mathbf{h}_P^-(\mathbf{x}')]\,\mathbf{h}_Q^+(\mathbf{x}'), \quad (6)$$

where $R_{PQ}(\theta(\mathbf{x}'))$ is the PWRC, $\theta(\mathbf{x}')$ is the incidence angle, and $\mathbf{h}_P^-(\mathbf{x}')$ and $\mathbf{h}_Q^+(\mathbf{x}')$ are the unit polarization vectors of the incident P-wave and the reflected PQ-wave, respectively. This approach, which is based on the geometrical-seismics approximation, assumes that the wavefront curvature at the reflector can be ignored, the reflector is plane, and the medium near the reflector is homogeneous. However, equation 6 is adequate only for subcritical incidence angles (if the frequency is sufficiently high) and causes artificial diffractions because of the discontinuous slope of the PWRC at the critical angle, as discussed by Kampfmann (1988), Wenzel et al. (1990), and Sen and Frazer (1991). These papers provide modeling examples that clearly show the drawbacks of using PWRCs in Kirchhoff modeling.

For a plane interface between homogeneous media, the wavefront curvature can be taken into account by representing the incident wave in the form of the Weyl integral over plane waves (Aki and Richards, 2002; Tsvankin, 1995). Each elementary plane wave in the integrand is multiplied by the corresponding PWRC to obtain an exact integral expression for the reflected wavefield.

To handle curved reflectors in heterogeneous media, Klem-Musatov et al. (2004) introduce a rigorous theory of reflection and transmission for interfaces of arbitrary shape in acoustic models. They show that the boundary data in the acoustic Kirchhoff integral can be represented by a generalized plane-wave decomposition called the

"reflection operator." This decomposition is local and must be evaluated separately for each individual point at the interface. Ayzenberg et al. (2007) prove that the exact action of the reflection operator on the incident wavefield can be approximately described by multiplying the incident wavefield by the corresponding ERC for each point at the interface. This formalism incorporates the local interface curvature into the reflection response and is not limited to small incidence angles and weak parameter contrasts across the reflector.

Here we extend the reflection operator to curved interfaces between isotropic and TI media. In Appendix B, we demonstrate that in the immediate vicinity of a curved interface, there exist local solutions of the wave equation in the form of generalized plane waves. Using these solutions as the basis, in Appendix C we introduce spectral integrals that describe the decomposition of the displacement field into the generalized plane P-, S_1-, and S_2-waves propagating to and from the interface. These generalized spectral integrals satisfy the boundary conditions (i.e., the continuity of displacement and traction across the interface) and are invariant with respect to the interface shape. In Appendix D, we represent the boundary conditions through reflection and transmission operators for anisotropic media.

As shown in Appendix D, the generalized plane-wave decomposition for the displacement component j of the PQ-mode reflected from a curved interface can be written as

$$u_{\mathrm{PQ},j}(s_1,s_2,0;\mathbf{x}') = \frac{\omega^2}{2\pi}\int_{-\infty}^{+\infty}\int_{-\infty}^{+\infty} R_{\mathrm{PQ}}(p;\mathbf{x}')\frac{h^{+}_{\mathrm{Q},j}(\mathbf{x}')}{h^{-}_{\mathrm{P},j}(\mathbf{x}')} \times u^{\mathrm{inc}}_{\mathrm{P},j}(p_1,p_2,0;\mathbf{x}')e^{i\omega(p_1s_1+p_2s_2)}dp_1dp_2, \tag{7}$$

where (s_1,s_2) are the curvilinear Chebychev coordinates that cover the interface S, (p_1,p_2) are the projections of the slowness vector onto the plane tangential to the interface at point $\mathbf{x}'$, $p=\sqrt{p_1^2+p_2^2}$, $R_{\mathrm{PQ}}(p;\mathbf{x}')$ is the PWRC at point $\mathbf{x}'$, and $h^{-}_{\mathrm{P},j}(\mathbf{x}')$ and $h^{+}_{\mathrm{Q},j}(\mathbf{x}')$ are the components of the unit polarization vectors of the incident P-wave and reflected PQ-wave, respectively. Graebner (1992) and Rüger (2002) give the exact PWRC $R_{\mathrm{PQ}}(p;\mathbf{x}')$ for a plane interface between two VTI media. In Appendix E, we reproduce the derivation of the amplitude-normalized PWRC in our notation and correct typos in the published solutions.

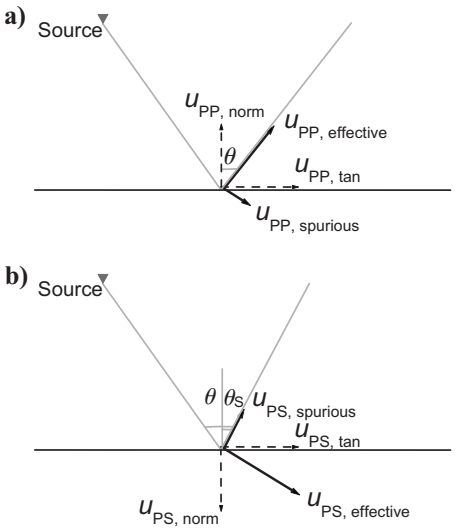

Figure 2. Effective and spurious components of (a) the reflected PP-wave and (b) the PS-wave. The ERC is defined through the projection of the displacement vector onto the geometrical polarization direction (see Appendix F).

For arbitrary interface geometry, the spectrum $\mathbf{u}^{\mathrm{inc}}_{\mathrm{P}}(p_1,p_2,0;\mathbf{x}')$ of the incident wave must be evaluated using the Fourier transform in the Chebychev coordinates (s_1,s_2):

$$\mathbf{u}^{\mathrm{inc}}_{\mathrm{P}}(p_1,p_2,0;\mathbf{x}') = \frac{1}{2\pi}\int_{-\infty}^{+\infty}\int_{-\infty}^{+\infty}\mathbf{u}^{\mathrm{inc}}_{\mathrm{P}}(s_1,s_2,0;\mathbf{x}') \times e^{-i\omega(p_1s_1+p_2s_2)}ds_1ds_2. \tag{8}$$

The generalized plane-wave decomposition in equation 7 is local and must be computed at each point $\mathbf{x}'$. It is valid within an infinitely thin layer near the interface and can be used only for calculating the reflection response in the immediate vicinity of the reflector.

In the special case of a plane interface, equation 7 reduces to the known Weyl integral over conventional plane waves (Tsvankin, 1995; Aki and Richards, 2002). For a horizontal reflector, the curvilinear coordinates (s_1,s_2) coincide with the ordinary Cartesian coordinates (x_1,x_2). Also, the spectrum $\mathbf{u}^{\mathrm{inc}}_{\mathrm{P}}(p_1,p_2,0;\mathbf{x}')$ of the incident wave in equation 8 is a known analytic function that does not depend on position $\mathbf{x}'$.

If the reflector is curved, numerical evaluation of the decomposition in equation 7 is prohibitively expensive, particularly because the spectrum $\mathbf{u}^{\mathrm{inc}}_{\mathrm{P}}$ must be computed locally in the curvilinear coordinates. To avoid the fourfold integration in equations 7 and 8, we propose an approximate solution for the reflected wavefield $u_{\mathrm{PQ},j}(s_1,s_2,0;\mathbf{x}')$ by representing it in a form similar to the geometrical-seismics approximation in equation 6. However, instead of the PWRCs used in equation 6, we introduce the ERCs as the ratios of the displacements of the reflected PQ-wave (projected onto the reflected ray; see Figure 2) and the incident P-wave (Appendix F):

$$\chi_{\mathrm{PP}}(\mathbf{x}') = \frac{u_{\mathrm{PP,norm}}(\mathbf{x}')\cos\,\theta(\mathbf{x}') + u_{\mathrm{PP,tan}}(\mathbf{x}')\sin\,\theta(\mathbf{x}')}{\left(ik_{\mathrm{P}}-\frac{1}{R}\right)\frac{e^{ik_{\mathrm{P}}R}}{R}}, \tag{9}$$

and

$$\chi_{\mathrm{PS}}(\mathbf{x}') = \frac{-u_{\mathrm{PS,norm}}(\mathbf{x}')\sin\,\theta_{\mathrm{S}}(\mathbf{x}') + u_{\mathrm{PS,tan}}(\mathbf{x}')\cos\,\theta_{\mathrm{S}}(\mathbf{x}')}{\left(ik_{\mathrm{P}}-\frac{1}{R}\right)\frac{e^{ik_{\mathrm{P}}R}}{R}}. \tag{10}$$

The reflection S-wave angle $\theta_{\mathrm{S}}(\mathbf{x}')$ is obtained from Snell's law as $\theta_{\mathrm{S}}(\mathbf{x}') = \sin^{-1}[(V^{(1)}_{\mathrm{S}}/V^{(1)}_{\mathrm{P}})\sin\,\theta(\mathbf{x}')]$. As demonstrated in Appendix F, the division by the displacement of the incident wave in equations 9 and 10 helps approximately compute the ERCs for an apparent plane reflector located at distance R^* from the source (Figure 3):

$$\chi_{PP}(\theta(\mathbf{x}'),L(\mathbf{x}')) = \frac{u^*_{PP,norm}(\mathbf{x}')\cos\,\theta(\mathbf{x}') + u^*_{PP,tan}(\mathbf{x}')\sin\,\theta(\mathbf{x}')}{\left(ik_P - \frac{1}{R^*}\right)\frac{e^{ik_P R^*}}{R^*}}, \quad (11)$$

$$\chi_{PS}(\theta(\mathbf{x}'),L(\mathbf{x}')) = \frac{-u^*_{PS,norm}(\mathbf{x}')\sin\,\theta_S(\mathbf{x}') + u^*_{PS,tan}(\mathbf{x}')\cos\,\theta_S(\mathbf{x}')}{\left(ik_P - \frac{1}{R^*}\right)\frac{e^{ik_P R^*}}{R^*}}, \quad (12)$$

and

$$R^*(\mathbf{x}') = R(\mathbf{x}')\frac{2-\sin^2\,\theta(\mathbf{x}')}{2-\sin^2\,\theta(\mathbf{x}') - 2R(\mathbf{x}')H(\mathbf{x}')\cos\,\theta(\mathbf{x}')}, \quad (13)$$

where $R(\mathbf{x}')$ is the distance between the source and point $\mathbf{x}'$ at the interface, $H(\mathbf{x}')$ is the mean interface curvature, and $L(\mathbf{x}') = \omega R^*(\mathbf{x}')/V_P^{(1)}$ is a dimensionless, frequency-dependent parameter (Ayzenberg et al., 2007). The reflected wavefield in equations 11 and 12 is computed from the Fourier-Bessel integrals for the apparent plane interface (Brekhovskikh, 1980; Aki and Richards, 2002):

$$u^*_{PQ,norm}(\mathbf{x}') = \omega^2\int_0^{+\infty} R_{PQ}(p)\frac{h^+_{Q,norm}}{h^-_{P,norm}}e^{i\omega l p_{P3}}J_0(r\omega p)pdp,$$

$$u^*_{PQ,tan}(\mathbf{x}') = -\omega^2\int_0^{+\infty} R_{PQ}(p)\frac{h^+_{Q,tan}}{h^-_{P,tan}}\frac{ie^{i\omega l p_{P3}}}{p_{P3}}J_1(r\omega p)p^2dp. \quad (14)$$

Here $J_0(r\omega p)$ and $J_1(r\omega p)$ are the zero-order and first-order Bessel functions, respectively, $p_{P3} = \sqrt{[V_P^{(1)}]^{-2} - p^2}$ is the vertical P-wave slowness, $l = R^*(\mathbf{x}')\cos\,\theta(\mathbf{x}')$, and $r = R^*(\mathbf{x}')\sin\,\theta(\mathbf{x}')$. For the reflected PP-wave, $h^+_{P,norm}/h^-_{P,norm} = -1$ and $h^+_{P,tan}/h^-_{P,tan} = 1$. For the PS-wave, $h^+_{S,norm}/h^-_{P,norm} = (V_S^{(1)}p)/(V_P^{(1)}p^{(1)}_{P3})$, $h^+_{S,tan}/h^-_{P,tan} = (V_S^{(1)}p^{(1)}_{S3})/(V_P^{(1)}p)$, and $p_{S3} = \sqrt{[V_S^{(1)}]^{-2} - p^2}$ is the vertical S-wave slowness.

Then, for a typical seismic-frequency range, the reflected wavefield near the interface (equation 7) can be expressed in the following form that is similar to the geometrical-seismics equation 6:

$$\mathbf{u}_{PQ}(\mathbf{x}') \simeq \chi_{PQ}(\theta(\mathbf{x}'),L(\mathbf{x}'))[\mathbf{u}^{inc}_P(\mathbf{x}')\cdot\mathbf{h}^-_P(\mathbf{x}')]\mathbf{h}^+_Q(\mathbf{x}'), \quad (15)$$

with the effective reflection coefficient χ_{PQ} determined by equations 11 and 12. Evaluation of the displacement $\mathbf{u}_{PQ}$ using equation 15 involves computing the single Fourier-Bessel integrals 14 instead of the fourfold integrals 7 and 8, which makes ERC-based diffraction modeling feasible.

The ERCs defined in equations 11 and 12 generalize the PWRC used in equation 6 by taking into account the curvatures of the incident wavefront and the reflector. Whereas PWRCs depend only on the stiffness and density contrasts across the boundary and the incidence angle $\theta(\mathbf{x}')$, the ERCs also are controlled by the dimensionless parameter $L(\mathbf{x}')$, which incorporates the interface curvature. In the zero-order stationary-phase approximation applied to homogeneous incident waves (Tsvankin, 1995), ERCs reduce to the corresponding PWRCs. In contrast to the PWRCs, the ERCs correctly describe reflection phenomena at near-critical and postcritical incidence angles (see the numerical examples below).

Equation 13 shows how the local reflector curvature is incorporated into the ERCs. If the reflector is locally plane, then $H(\mathbf{x}') = 0$ and the apparent distance $R^*(\mathbf{x}')$ coincides with $R(\mathbf{x}')$. For particular parameter combinations, $R^*(\mathbf{x}')$ may go to infinity, which means that the incident P-wave appears to be locally plane; in that case, the ERC reduces to the PWRC. For certain values of the product $R(\mathbf{x}')H(\mathbf{x}')$, the distance $R^*(\mathbf{x}')$ may become negative. Then the apparent source represents the focus of an apparent converging spherical wave, and the ERC becomes complex conjugate.

PARAMETER SENSITIVITY STUDY AND 3D DIFFRACTION MODELING

Numerical study of ERCs

As follows from the formalism discussed above, ERCs provide a practical approximate tool for computing the reflected wavefield at a curved reflector for a typical seismic-frequency range. Here, we study the ERCs for an interface between isotropic and TI media as a function of the parameter L, Thomsen anisotropy parameters of the reflecting half-space, and the local interface geometry incorporated into the apparent distance R^*. If the reflected wavefield is well described by geometrical seismics, the ERCs reduce to the corresponding PWRCs. Therefore, the difference between the effective and plane-wave reflection coefficients helps estimate the error of the geometrical-seismics approximation.

Influence of L

First, we examine the dependence of ERCs computed for a plane interface on the parameter $L = \omega R^*/V_P^{(1)}$ (where ω is the angular frequency and R^* is the distance from the apparent source to point $\mathbf{x}'$ at the interface). Figure 4 compares the ERCs for PP- and PS-waves computed for a wide range of L with the corresponding PWRCs. For

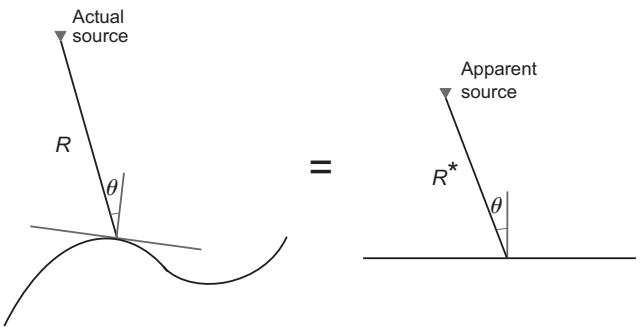

Figure 3. ERCs for a curved reflector can be approximately computed for an apparent plane reflector located at distance R^* from the source. The incidence angle θ remains the same.

both modes, the difference between the ERCs and PWRCs decreases for larger values of L (i.e., for larger frequency ω or distance R^*). However, in contrast to PWRCs, ERCs oscillate in the postcritical domain even for $L = 10^3$ because of the interference of the reflected and head waves.

For the relatively small $L = 10$, the ERC (especially the one for PS-waves) deviates substantially from the PWRC, even at subcritical incidence angles. This means that for low values of L, geometrical-seismics approximations can be used only for near-vertical incidence (i.e., small source-receiver offsets). Indeed, it is well known that the accuracy of the geometrical-seismics approximation strongly depends on the source-interface distance normalized by the predominant wavelength (Tsvankin, 1995). If the source (in our case, the apparent source) is close to the interface, the reflected wavefield is influenced by the curvature of the incident wavefront and cannot be accurately described by geometrical-seismics expressions.

Influence of the anisotropy parameters

The contribution of the anisotropy parameters ε and δ to the ERCs for PP- and PS-waves increases at near- and postcritical incidence angles (Figures 5 and 6). The critical angle is controlled by the horizontal P-wave velocity in the TI medium that depends on $\varepsilon(V_P^{(2)}(90) = V_{P0}^{(2)}\sqrt{1+2\varepsilon})$. Figures 5a and 6a confirm that the critical angle decreases for larger values of ε, which causes a horizontal shift of the ERC curves. Also, the PS-wave ERC in the postcritical domain increases noticeably with ε. In general, the reflectivity of PS-waves is more sensitive to the anisotropy parameters than is that of PP-waves, likely because shear-wave signatures are controlled primarily by the relatively large parameter $\sigma[\sigma = (V_{P0}^{(2)}/V_{S0}^{(2)})^2(\varepsilon - \delta)]$. Typically, the magnitude of σ exceeds $|\varepsilon|$ and $|\delta|$ significantly; in our model, σ varies from -2.94 to 2.94.

Because ERCs at postcritical incidence angles include the contributions of the reflected waves and the head waves, Figures 5 and 6 do not provide conclusive information to predict the influence of ε and δ on the time-domain wavefield. The long-offset synthetic seismograms discussed below help to separate the reflected and head waves and evaluate their dependence on the anisotropy parameters of the reflecting medium.

Influence of the reflector shape

Here, we generate ERCs for a curved interface that has a flexural shape governed by the parameter Δz (Figure 7). When the reflector degenerates into a horizontal plane ($\Delta z = 0$), the apparent distance R^* reduces to the actual source-reflector distance R, which has no singular points. The offset dependence of R^* becomes more complicated with increasing reflector curvature (Figure 7b).

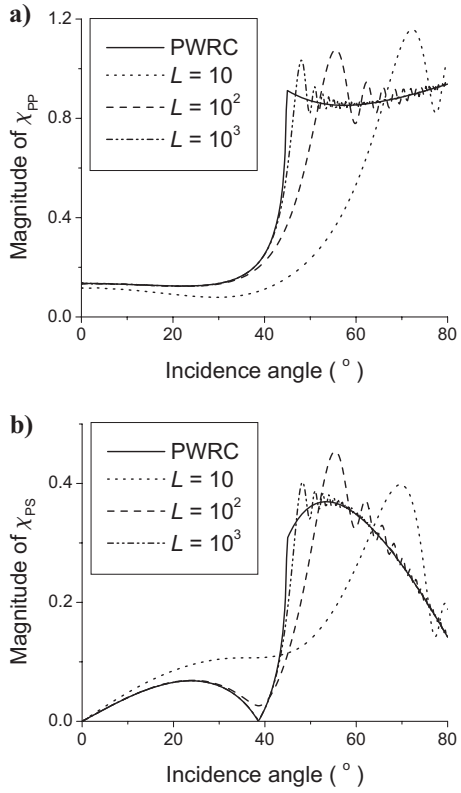

Figure 4. Dependence of the magnitude of the (a) PP-wave and (b) PS-wave ERCs on the parameter L. The corresponding PWRCs are shown for comparison. The reflector is a horizontal plane 1 km below the source. The parameters of the incidence isotropic medium are $V_P^{(1)} = 2$ km/s, $V_S^{(1)} = 1.2$ km/s, and $\rho^{(1)} = 2.15$ g/cm^3; for the reflecting TI medium, they are $V_{P0}^{(2)} = 2.4$ km/s, $V_{S0}^{(2)} = 1.4$ km/s, $\rho^{(2)} = 2.35$ g/cm^3, $\varepsilon = 0.2$, and $\delta = 0.1$.

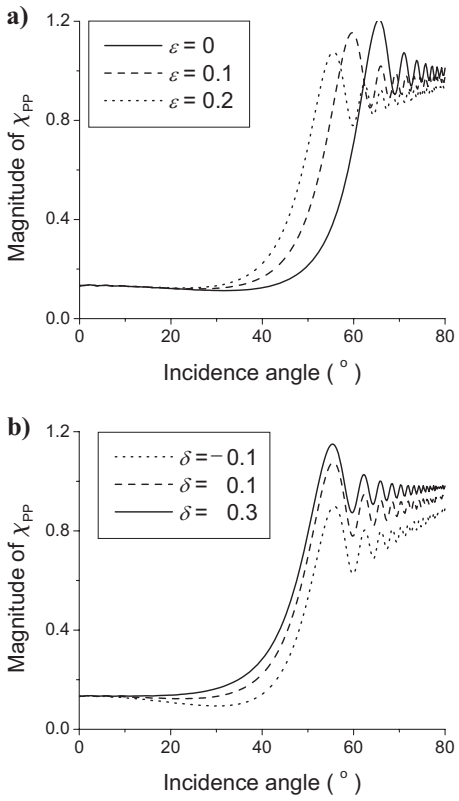

Figure 5. Dependence of the PP-wave ERC on the anisotropy parameters. (a) $\delta = 0.1$ and $\varepsilon = 0$, 0.1, and 0.2; (b) $\varepsilon = 0.2$ and $\delta = -0.1$, 0.1, and 0.3. The interface is a horizontal plane 1 km below the source. The medium parameters are $V_P^{(1)} = 2$ km/s, $V_S^{(1)} = 1.2$ km/s, $\rho^{(1)} = 2.15$ g/cm^3, $V_{P0}^{(2)}$=2.4 km/s, $V_{S0}^{(2)} = 1.4$ km/s, $\rho^{(2)} = 2.35$ g/cm^3; the frequency f is 32 Hz.

Figure 8 displays the ERCs for PP- and PS-waves for three values of Δz. We observe a rapid change in both ERCs near an offset of 0.75 km, where the distance R^* exhibits sharp spikes associated with the flexural segment of the reflector.

Tip-wave superposition method for elastic media

To model reflected wavefields for curved interfaces, we evaluate the tip-wave beams (equations 3 and 5) for PP- and PS-waves. We obtain the seismic-frequency approximation of the integral using TWSM (Klem-Musatov and Aizenberg, 1985; Klem-Musatov et al., 1993, 2008). The published version of the method is designed for modeling 3D wavefields in layered acoustic media with complex interface geometries. The main assumption of the method is that the source-interface, receiver-interface, and interface-interface distances obey the Rayleigh principle (i.e., they are of the order of several wavelengths or larger).

In Appendix A, we extend TWSM to elastic isotropic media because the upper half-space in our model is isotropic. The TWSM generates the reflection response by superposition of tip-diffracted waves excited at the reflector in accordance with Huygens' principle. As Figure 9 shows, a tip-wave beam is formed by the reflected wave, four edge-diffracted waves, and eight tip-diffracted waves. The tip-diffracted waves make the most prominent contribution to the beam, which explains the method's name.

Our implementation of TWSM involves splitting the reflector into rhombic elements that conform to the Chebychev coordinates introduced earlier. Each element acts as a secondary source emitting a tip-wave beam toward the receiver array, and the beams form the "receiver matrix." We compute the boundary data using the ERC or the PWRC, and form the source matrix for all rhombic elements at the interface. Then we multiply the two matrices element by element to generate the reflected wavefield and sum the reflection responses at each receiver.

TWSM uses specific approximations of the surface propagators and the reflection and transmission operators for the seismic-frequency range. Our implementation of the propagators is based on the Fresnel approximation in the coordinate domain. Implementation of the reflection and transmission operators is based on a boundary-layer approximation in the domain of spatial frequencies. Both approximations cause negligible errors within the seismic-frequency range. The error in the ERCs increases for high frequencies, and the error in the tip-wave beam approximations increases for low frequencies. Ayzenberg et al. (2007) discuss the accuracy of TWSM. Where possible, we use independent methods to show that TWSM produces correct traveltimes and the amplitude error does not exceed a few percent. In particular, for plane reflectors, we used reflectivity modeling for a trace-by-trace comparison of the modeling results.

With PWRCs, TWSM is inexpensive computationally but requires storage of large matrices that contain information about tip waves. Although storing the data might present a logistical problem, it allows minor changes to the model to be incorporated without recalculating all tip-wave beams. This advantage of TWSM becomes particularly valuable for layered models and in survey design. Appli-

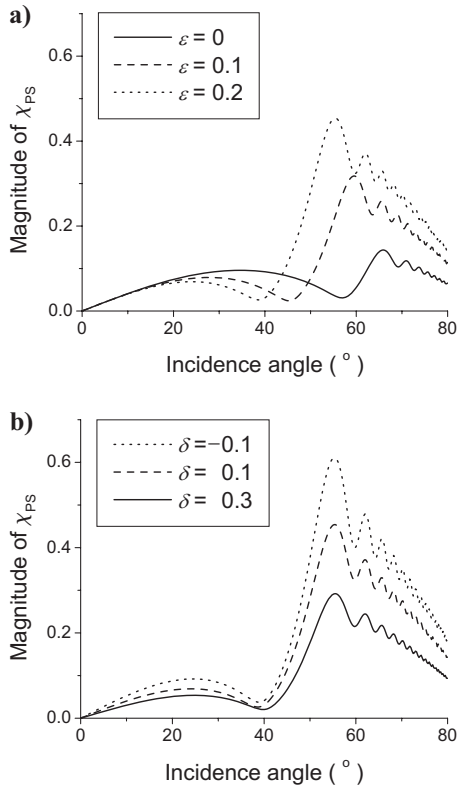

Figure 6. Dependence of the PS-wave ERC on the anisotropy parameters for the model from Figure 5. Plot (a) shows the influences of ε and plot (b) the influence of δ.

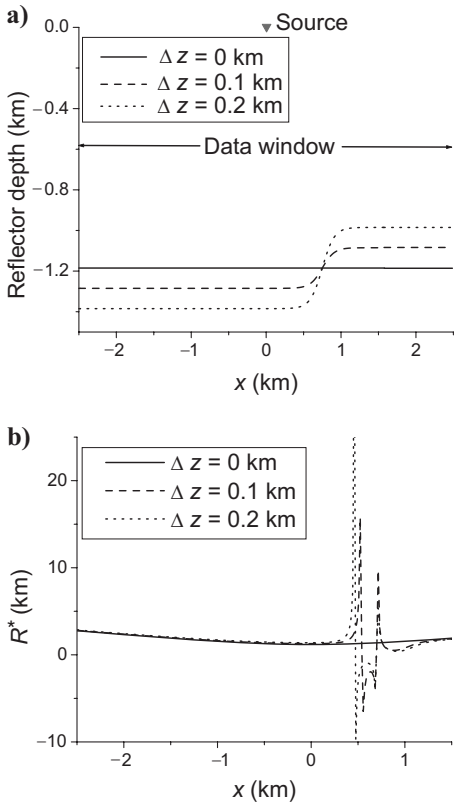

Figure 7. (a) Model with a curved reflector. (b) The corresponding apparent distance R^*. The source is at the surface and an array of 101 receivers is at a depth of 585 m with a 50-m step. The reflector is described by the equation $x_3 = -1.185 + \Delta z \tanh[2\pi(x_1 - 0.75)]$. The parameter Δz is marked on the plot.

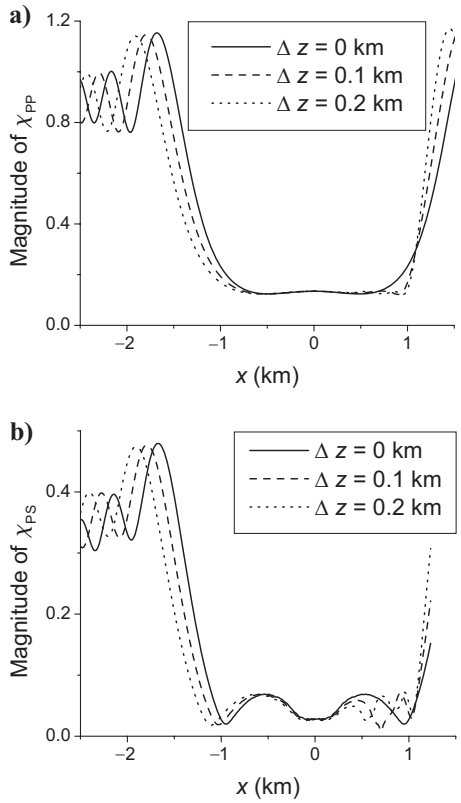

Figure 8. Offset-dependent magnitude of the (a) PP-wave and (b) PS-wave ERCs for the model from Figure 7. The medium parameters are $V_P^{(1)} = 2$ km/s, $V_S^{(1)} = 1.2$ km/s, $\rho^{(1)} = 2.15$ g/cm^3, $V_{P0}^{(2)} = 2.4$ km/s, $V_{S0}^{(2)} = 1.4$ km/s, $\rho^{(2)} = 2.35$ g/cm^3, $\varepsilon = 0.2$, and $\delta = 0.1$.

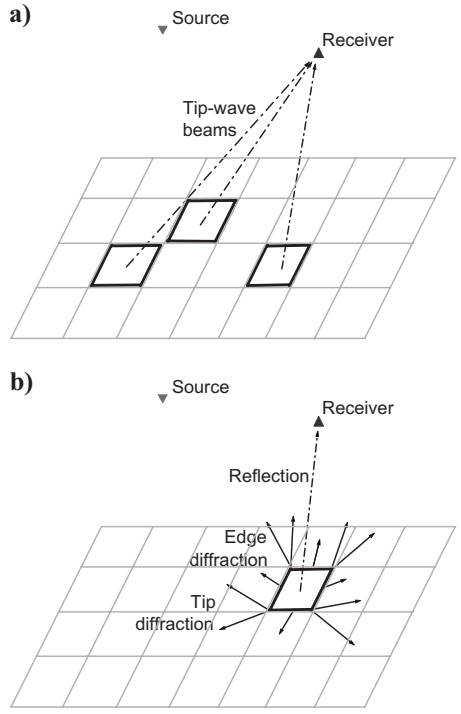

Figure 9. (a) Tip-wave beam interference at the receiver. (b) Each tip-wave beam contains the main reflection, four edge-diffracted waves, and eight tip-diffracted waves.

cation of ERCs in TWSM involves computing the Fourier-Bessel integrals for the entire frequency range of the initial wavelet instead of the simple, closed-form PWRC expressions. Also, disk-space requirements become even more demanding because the tip-wave matrices must be stored separately for each frequency.

Having introduced our implementation of TWSM, we now briefly review the main limitations of our modeling methodology. First, the current version of the algorithm does not account for multiple scattering at curved reflectors. Second, we assume that the medium does not contain shadow zones in which geometrical rays do not propagate. Modeling reflections in such zones would involve generalizing tip-wave beams for areas in which the reflected wavefield is formed by the diffracted incident wave. Third, the seismic-frequency approximation used to combine TWSM with ERCs loses its accuracy for short (relative to the wavelength) distances between the reflector and the receivers.

Modeling results

As the numerical tests above illustrate, ERCs are sensitive to the elastic parameters and the shape of the interface. Here, we combine ERCs with TWSM to generate the time-domain wavefield and analyze its behavior for different reflector shapes.

In all numerical tests below, we use the Puzyrev wavelet:

$$F(t) = -e^{-p^2/\pi^2} \sin p, \quad p = 2\pi \frac{t - t_0}{T}, \tag{16}$$

where $T = 0.032$ s is the period and $t_0 = 0.064$ s (Figure 10).

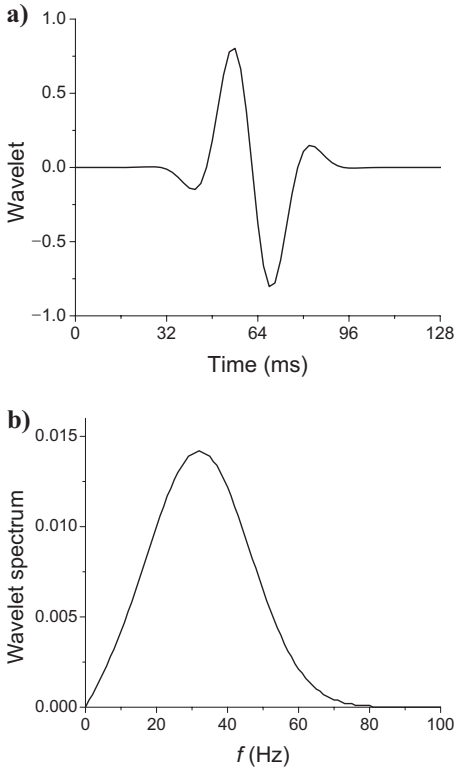

Figure 10. (a) Puzyrev wavelet and (b) its spectrum. The dominant period is 0.032 s, and the dominant frequency is 32 Hz.

Influence of anisotropy parameters

The seismograms in Figures 11–14 are computed for a curved reflector described by the function $x_3 = -1 + 0.3\exp(-8x_1^2 - 8x_2^2)$. The reflector has a 0.3-km-high Gaussian-shaped anticline directly below the source. The reflection traveltimes of PP- and PS-waves exhibit a wide triplication (cusp) at the far offsets, which corresponds to the caustic produced at the anticlinal part of the reflector. We observe slight aliasing at small offsets because of the element size. There also is a weak coherent artifact formed by two diffracted waves interfering on the zero-offset trace. This artifact is generated at the edges of the model and is not suppressed completely by the absorbing boundaries, which are designed to diminish the edge effects (Ayzenberg et al., 2007).

In agreement with the ERC in Figure 5a, the PP-wave reflection amplitude at long offsets rapidly increases with ε (Figure 11). The amplitude at the largest offset (2.5 km) is approximately four times higher for $\varepsilon = 0.2$ than for $\varepsilon = 0$. In contrast, the near-offset reflections are weakly sensitive to ε. The influence of δ on PP-wave amplitudes is most visible at moderate offsets between 1.5 and 1.7 km (Figure 12). For the maximum offset, the amplitude increases approximately by 15% when δ increases by 0.2. However, the near-offset reflections are almost insensitive to δ.

Figures 13 and 14 show the PS wavefield for a range of ε and δ values. The influence of both anisotropy parameters on the reflected

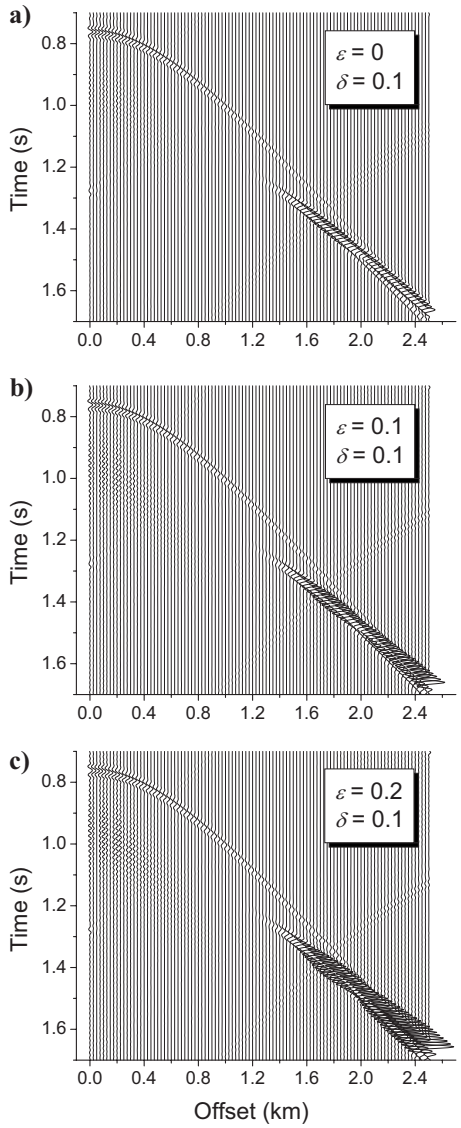

Figure 11. Influence of ε on the vertical displacement of the PP-wave reflected from a curved interface. The source and an array of 101 receivers are placed at the surface. The reflector is described by $x_3 = -1 + 0.3\exp(-8x_1^2 - 8x_2^2)$, so that the cap of the Gaussian anticline is at a depth of 0.7 km below the source. The medium parameters are $V_P^{(1)} = 2$ km/s, $V_S^{(1)} = 1.2$ km/s, $\rho^{(1)} = 2.15$ g/cm^3, $V_{P0}^{(2)} = 2.4$ km/s, $V_{S0}^{(2)} = 1.4$ km/s, $\rho^{(2)} = 2.35$ g/cm^3; the values of ε and δ are marked on the plots.

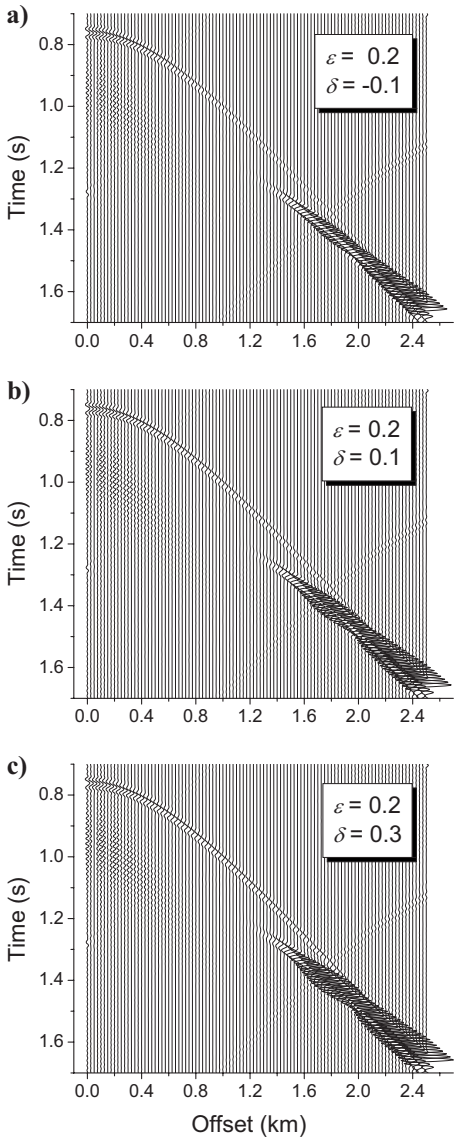

Figure 12. Influence of δ on the PP-wave vertical displacement for the model from Figure 11.

wave can be predicted from the corresponding ERC in Figure 6. In particular, the moderate- and far-offset reflection amplitudes increase noticeably with ε. The amplitude at the largest offset becomes six to eight times higher when ε changes from zero to 0.1, and two times higher when ε changes from 0.1 to 0.2. Interestingly, for the same change in ε, the amplitude of the PPS head wave decreases only by a factor of four. (Because it has a very small amplitude, we mark its arrival on the rightmost trace with an arrow.) Although the influence of δ is less pronounced, a 0.4 increase in δ reduces the maximum-offset amplitude of the reflected PS-wave and the head wave by 50%.

Influence of the reflector shape

Figure 15 displays synthetic PP-wave seismograms computed for a flexural reflector with variable mean curvature (Figure 7). Hanyga

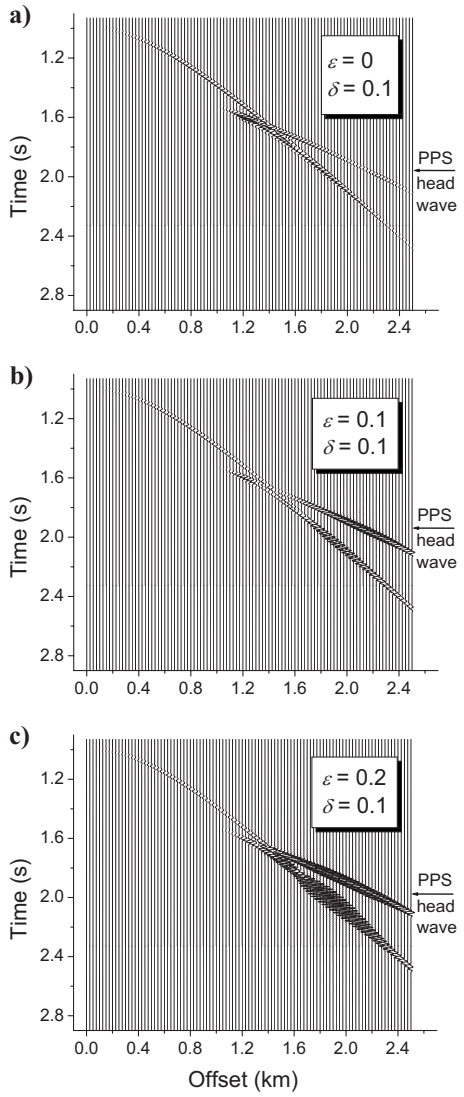

Figure 13. Influence of ε on the PS-wave vertical displacement for the model from Figure 11. The head-wave arrival on the rightmost trace is marked with an arrow.

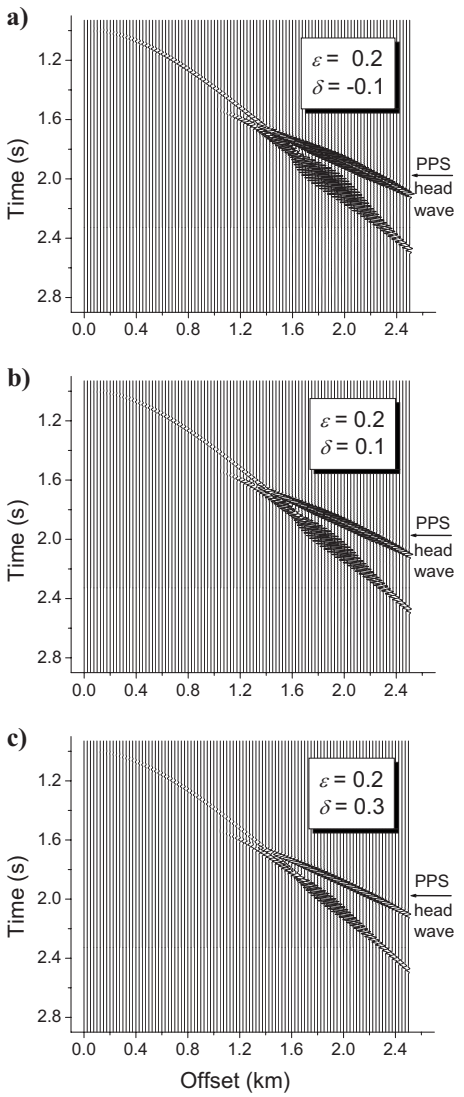

Figure 14. Influence of δ on the PS-wave vertical displacement for the model from Figure 11. The head-wave arrival on the rightmost trace is marked with an arrow.

and Helle (1995) use the isotropic 2D version of this model to test finite-difference and generalized ray-tracing algorithms. As the value of Δz increases, the flexure produces a strong caustic loop formed near zero offset. The head waves cannot be identified clearly because of the limited length of the receiver array, which extends only to the interference zone of the reflected and head waves.

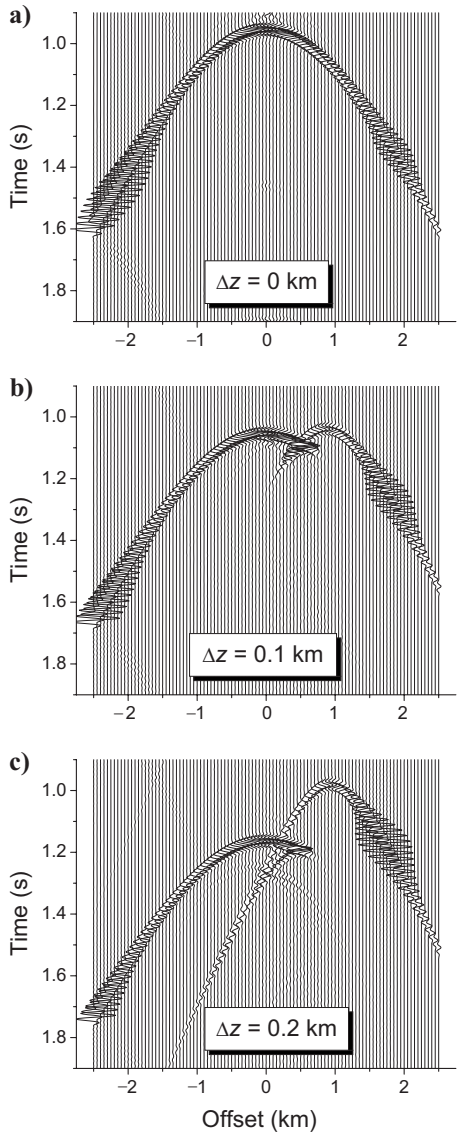

Figure 15. PP-wave vertical displacement computed with the ERCs for the model from Figures 7 and 8. The source is placed at the surface and an array of 101 receivers is located at a depth of 585 m with a 50-m step. The reflector is described by the equation $x_3 = -1.185 + \Delta z \tanh[2\pi(x_1 - 0.75)]$; the parameter Δz is marked on the plots. The medium parameters are $V_P^{(1)} = 2$ km/s, $V_S^{(1)} = 1.2$ km/s, $\rho^{(1)} = 2.15$ g/cm^3, $V_{P0}^{(2)} = 2.4$ km/s, $V_{S0}^{(2)} = 1.4$ km/s, $\rho^{(2)} = 2.35$ g/cm^3, $\varepsilon = 0.2$, and $\delta = 0.1$.

For a plane reflector ($\Delta z = 0$), we compared our modeling results with the exact wavefield computed by the reflectivity method. As expected, the elastic version of TWSM based on the superposition of tip-wave beams accurately reproduces traveltimes for the whole offset range. The amplitudes in Figure 15 are only a few percent higher than those produced by the reflectivity algorithm.

To evaluate the errors of the conventional Kirchhoff modeling technique, we also computed the wavefield using the PWRC in TWSM (Figure 16). The discontinuous slope of the PWRC at the

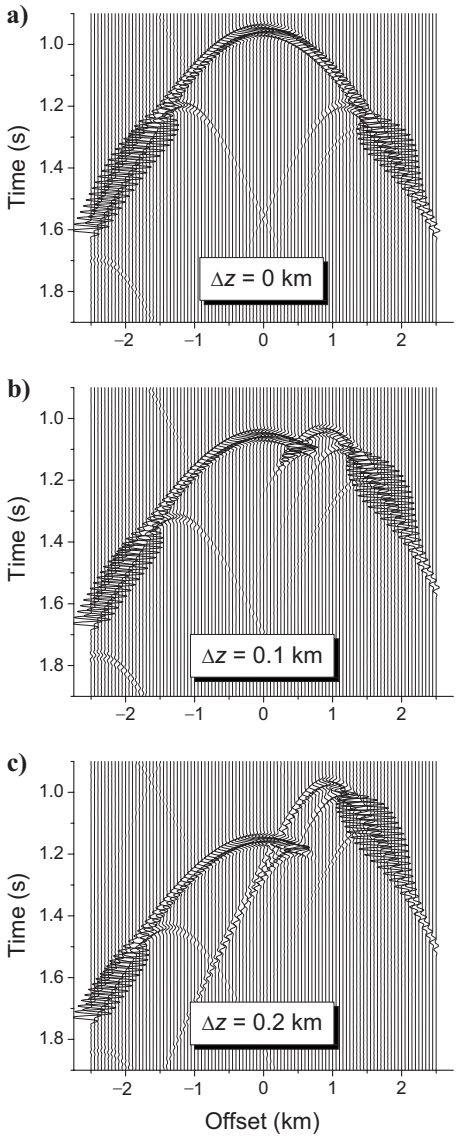

Figure 16. PP-wave vertical displacement computed with the PWRC for the model from Figure 15.

critical angles causes artificial diffractions for plane ($\Delta z = 0$) and curved reflectors. Additionally, the reflection amplitudes for near- and postcritical offsets are higher than those obtained with the ERC in Figure 15.

Similar conclusions can be drawn from the PS-wave seismograms for the same model in Figures 17 and 18. The PS reflection also exhibits a caustic loop that becomes more prominent for $\Delta z = 0.2$ km. The critical offset for the converted (PPS) head wave is smaller than that for the corresponding PPP-wave, which explains the separation of the head wave (marked with an arrow for the leftmost receiver) and reflected wave at the far offsets in Figure 17. Although the artificial diffractions caused by the PWRC in Figure 18 are less pronounced than those for PP-waves, application of the ERC (Figure 17) yields a cleaner gather.

Our 3D modeling results obtained with TWSM agree well kinematically with the wavefields computed by finite differences and generalized ray tracing for the corresponding isotropic 2D model (Hanyga and Helle, 1995). However, the amplitudes are not the same because of different geometrical spreading in two and three dimensions and the influence of anisotropy in our model.

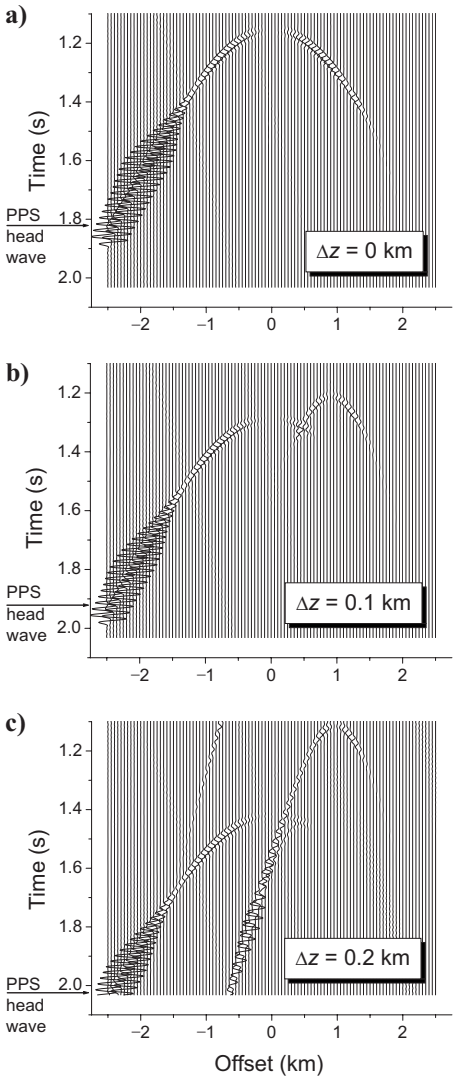

Figure 17. PS-wave vertical displacement computed with the ERCs for the model from Figure 15. The head-wave arrival on the leftmost trace is marked with an arrow.

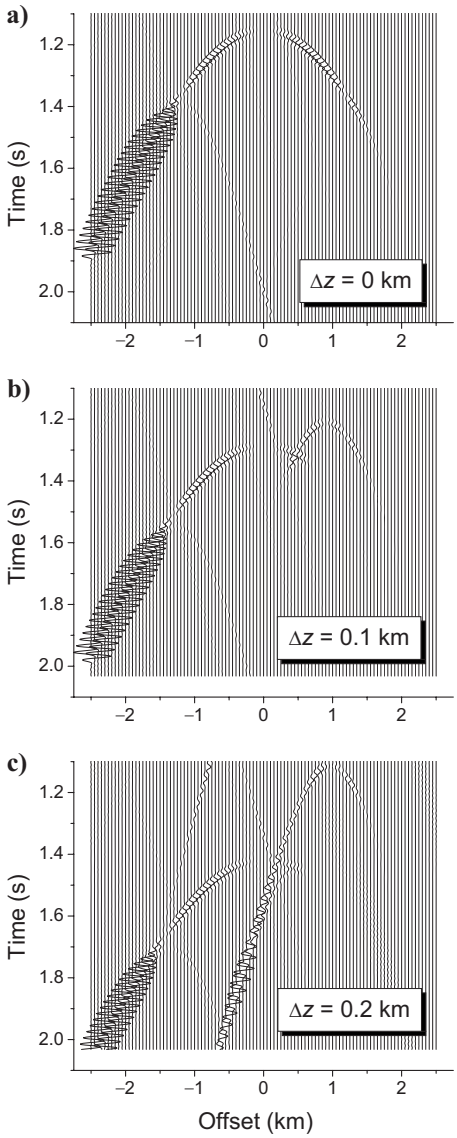

Figure 18. PS-wave vertical displacement computed with the PWRCs for the model from Figure 15.

CONCLUSIONS

Effective reflection coefficients (ERCs) provide a practical tool for modeling near- and postcritical reflected wavefields and for taking the interface curvature into account. By extending a formalism suggested previously for the acoustic problem, we gave a complete analytic description of ERCs for curved reflectors in anisotropic media. The reflected wavefield can be expressed through a generalized plane-wave decomposition, which includes the local spatial spectrum of the incident wave expressed through an integral over the whole interface.

Although this decomposition gives an accurate wavefield representation near a reflector of arbitrary shape, its computational cost for 3D anisotropic models is prohibitive. Therefore, we suggested obtaining the reflected wavefield approximately from the conventional Weyl-type integral computed for an apparent source location, which depends on the incidence angle and the mean reflector curvature. Then the ratio of the reflected and incident wavefields yields the spatially varying ERC along the reflector. To incorporate ERCs in 3D diffraction modeling, we used the tip-wave superposition method (TWSM), generalized for elastic wave propagation. The superposition of the tip-wave beams that correspond to rhombic interface segments produces correct reflection traveltimes, whereas the accuracy of amplitudes depends on the validity of the seismic-frequency approximation used in TWSM and in computing ERCs. TWSM also can model multipathing and caustics produced by curved segments of the reflector.

We implemented this formalism and studied the properties of ERCs for an interface separating isotropic and TI media. The symmetry axis in the reflecting TI half-space was assumed to be orthogonal to the reflector, which is typical for anisotropic shale layers. For the special case of a plane interface, the ERC represents the frequency-dependent exact wavefield governed by the velocity and density contrasts, Thomsen anisotropy parameters, and source-receiver geometry. Numerical tests show that the ERC for PP-waves at postcritical incidence angles is particularly sensitive to the parameter ε, responsible for near-horizontal P-wave propagation in the TI half-space.

The ERC deviates substantially from the corresponding plane-wave reflection coefficient (PWRC) in the postcritical domain, where the displacement field is influenced by the head wave. At low frequencies, the difference between ERC and PWRC can be significant even for subcritical incidence angles. These results confirm the limitations of the geometrical-seismics approximation, which is based on the PWRC, in describing point-source radiation in layered media.

Our synthetic examples illustrated the importance of properly accounting for the reflector curvature when computing ERCs. When the reflector is curved, the ERC can change rapidly along the interface in accordance with variations of the local interface shape, thus influencing synthetic modeling.

The methodology developed here can be used to generate accurate boundary data for 3D Kirchhoff modeling in anisotropic media. In particular, our synthetic examples confirm that ERCs eliminate the artifacts produced by PWRCs and provide more accurate amplitudes for large incidence angles and in the presence of significant reflector curvature. Our results also can be applied to anisotropic AVO analysis of long-offset PP and PS reflection data.

ACKNOWLEDGMENTS

Milana Ayzenberg is grateful to the Center for Wave Phenomena for support during her five-month visit to Colorado School of Mines. Arkady Aizenberg acknowledges the Russian Foundation for Basic Research (grant 07-05-00671). This work was partially funded by the Consortium Project on Seismic Inverse Methods for Complex Structures at the Center for Wave Phenomena.

APPENDIX A

TIP-WAVE SUPERPOSITION METHOD FOR ISOTROPIC ELASTIC MEDIA

Here, we generalize the tip-wave superposition method (TWSM) for elastic media to model the PP- and PS-wavefields reflected from a curved interface. First, we rewrite integral 1 in a form similar to equation 20 of Pao and Varatharajulu (1976):

$$\mathbf{u}(\mathbf{x}) = \rho^{(1)}[V_P^{(1)}]^2 \int\int_S [(\nabla' \cdot \mathbf{G})(\mathbf{u}\cdot\mathbf{n}') - (\mathbf{G}\cdot\mathbf{n}') \cdot(\nabla'\cdot\mathbf{u})]\, dS(\mathbf{x}') + \rho^{(1)}[V_S^{(1)}]^2 \int\int_S [(\mathbf{n}'\times\mathbf{u}) \cdot(\nabla'\times\mathbf{G}) + (\mathbf{n}'\times(\nabla'\times\mathbf{u}))\cdot\mathbf{G}]\, dS(\mathbf{x}'), \quad \text{(A-1)}$$

where $\nabla' = (\partial/\partial x', \partial/\partial y', \partial/\partial z')$ and $\mathbf{n}'$ is the normal to the reflector at point $\mathbf{x}'$. The reflected displacement field can be separated into the PP- and PS-modes (Ben-Menahem and Singh, 1998):

$$\mathbf{u}(\mathbf{x}) = \mathbf{u}_{\mathrm{PP}}(\mathbf{x}) + \mathbf{u}_{\mathrm{PS}}(\mathbf{x}), \quad \text{(A-2)}$$

which satisfy the equations

$$[V_{\mathrm{P}}^{(1)}]^2 \nabla[\nabla\cdot\mathbf{u}_{\mathrm{PP}}(\mathbf{x})] + \omega^2\mathbf{u}_{\mathrm{PP}}(\mathbf{x}) = 0 \quad \text{(A-3)}$$

and

$$-[V_{\mathrm{S}}^{(1)}]^2 \nabla\times[\nabla\times\mathbf{u}_{\mathrm{PS}}(\mathbf{x})] + \omega^2\mathbf{u}_{\mathrm{PS}}(\mathbf{x}) = 0. \quad \text{(A-4)}$$

Likewise, the Green's displacement tensor can be split into the P- and S-wave components:

$$\mathbf{G}(\mathbf{x}',\mathbf{x}) = \mathbf{G}_{\mathrm{P}}(\mathbf{x}',\mathbf{x}) + \mathbf{G}_{\mathrm{S}}(\mathbf{x}',\mathbf{x}), \quad \text{(A-5)}$$

where

$$\mathbf{G}_{\mathrm{P}}(\mathbf{x}',\mathbf{x}) = \frac{1}{\rho^{(1)}\omega^2}\nabla g_{\mathrm{P}}(\mathbf{x}',\mathbf{x})\nabla',$$

$$\mathbf{G}_{\mathrm{S}}(\mathbf{x}',\mathbf{x}) = \frac{1}{\rho^{(1)}\omega^2}\nabla\times[g_{\mathrm{S}}(\mathbf{x}',\mathbf{x})\mathbf{I}]\times\nabla' = \frac{1}{\rho^{(1)}\omega^2}\left[\frac{\omega^2}{[V_{\mathrm{S}}^{(1)}]^2} g_{\mathrm{S}}(\mathbf{x}',\mathbf{x})\mathbf{I} - \nabla g_{\mathrm{S}}(\mathbf{x}',\mathbf{x})\nabla'\right], \quad \text{(A-6)}$$

and

$$g_Q(\mathbf{x}',\mathbf{x}) = \frac{e^{i\omega R/V_Q^{(1)}}}{4\pi R}, \quad R = |\mathbf{x}-\mathbf{x}'|, \quad Q = P,S. \tag{A-7}$$

Substituting equations A-2 and A-5 into equation A-1, we obtain the reflected PP-wavefield as

$$\mathbf{u}_{PP}(\mathbf{x}) = \rho^{(1)}[V_P^{(1)}]^2 \int\int_S [(\nabla'\cdot\mathbf{G}_P)(\mathbf{u}_{PP}\cdot\mathbf{n}') - (\mathbf{G}_P\cdot\mathbf{n}')\cdot(\nabla'\cdot\mathbf{u}_{PP})]\,dS'. \tag{A-8}$$

For the PS-wavefield,

$$\mathbf{u}_{PS}(\mathbf{x}) = \rho^{(1)}[V_S^{(1)}]^2 \int\int_S [(\mathbf{n}'\times\mathbf{u}_{PS})\cdot(\nabla'\times\mathbf{G}_S) - ((\nabla'\times\mathbf{u}_{PS})\times\mathbf{n}')\cdot\mathbf{G}_S]\,dS'. \tag{A-9}$$

Next, we rewrite the terms involving G_P in equation A-8 (see details in Ben-Menahem and Singh, 1998; their section 4.1 and Appendix A):

$$\nabla'\cdot\mathbf{G}_P = -\nabla\cdot\mathbf{G}_P = -\frac{1}{\rho^{(1)}\omega^2}\Delta g_P\nabla' = \frac{1}{\rho^{(1)}[V_P^{(1)}]^2} g_P\nabla' = -\frac{1}{\rho^{(1)}[V_P^{(1)}]^2}\nabla g_P \tag{A-10}$$

and

$$\mathbf{G}_P\cdot\mathbf{n}' = \frac{1}{\rho^{(1)}\omega^2}\nabla g_P\nabla'\cdot\mathbf{n}' = \frac{1}{\rho^{(1)}[V_P^{(1)}]^2}\nabla[(\mathbf{n}'\cdot\nabla')g_P]. \tag{A-11}$$

Substituting equations A-10 and A-11 into equation A-8 yields

$$\mathbf{u}_{PP}(\mathbf{x}) = \nabla\int\int_S \left[\frac{\partial g_P(\mathbf{x}',\mathbf{x})}{\partial n'} d_{1,PP}(\mathbf{x}') - g_P(\mathbf{x}',\mathbf{x}) d_{2,PP}(\mathbf{x}')\right] dS(\mathbf{x}'), \tag{A-12}$$

where

$$d_{1,PP}(\mathbf{x}') = -\frac{[V_P^{(1)}]^2}{\omega^2}[\nabla'\cdot\mathbf{u}_{PP}(\mathbf{x}')],$$
$$d_{2,PP}(\mathbf{x}') = \mathbf{u}_{PP}(\mathbf{x}')\cdot\mathbf{n}'. \tag{A-13}$$

The terms $d_{1,PP}$ and $d_{2,PP}$ can be expressed through the incident wavefield and ERC χ_{PP} using approximation F-6:

$$d_{1,PP}(\mathbf{x}') \simeq -\frac{[V_P^{(1)}]^2}{\omega^2}\chi_{PP}(\mathbf{x}')\nabla'\cdot\{[\mathbf{u}_P^{inc}(\mathbf{x}')\cdot\mathbf{h}_P^-(\mathbf{x}')]\mathbf{h}_P^+(\mathbf{x}')\}$$
$$\simeq \chi_{PP}(\mathbf{x}')g_P^{inc}(\mathbf{x}',\mathbf{x}),$$
$$d_{2,PP}(\mathbf{x}') \simeq \chi_{PP}(\mathbf{x}')[\mathbf{u}_P^{inc}(\mathbf{x}')\cdot\mathbf{h}_P^-(\mathbf{x}')][\mathbf{h}_P^+(\mathbf{x}')\cdot\mathbf{n}'], \tag{A-14}$$

where $\mathbf{u}_P^{inc}(\mathbf{x}') = \nabla' g_P^{inc}(\mathbf{x}',\mathbf{x})$.

Because the integral in equation A-12 coincides with the acoustic surface integral 7 analyzed in Ayzenberg et al. (2007), we can use their methodology (TWSM) to split the reflector into small rhombic elements. To extend TWSM to elastic media, we represent the PP-wavefield (equation A-12) in a form similar to equations 11 and 12 from Ayzenberg et al. (2007):

$$\mathbf{u}_{PP}(\mathbf{x}) \simeq \sum_j \Delta\mathbf{B}_{PP[j]}(\mathbf{x}), \tag{A-15}$$

where $\Delta\mathbf{B}_{PP[j]}(\mathbf{x})$ is the vector contribution of the surface element $\Delta\Pi_{[j]}$:

$$\Delta\mathbf{B}_{PP[j]}(\mathbf{x}) = \frac{i\omega}{V_P^{(1)}}\mathbf{l}_{P[j]}(\mathbf{x})\int\int_{\Delta\Pi_{[j]}}\left[\frac{\partial g_P(\mathbf{x}',\mathbf{x})}{\partial n'} d_{1,PP}(\mathbf{x}') - g_P(\mathbf{x}',\mathbf{x}) d_{2,PP}(\mathbf{x}')\right] dS'; \tag{A-16}$$

$\Delta\Pi_{[j]}$ is the area of the surface element $\mathbf{l}_{P[j]}(\mathbf{x}) = \nabla g_P(\mathbf{x}'_{[j]},\mathbf{x})/|\nabla g_P(\mathbf{x}'_{[j]},\mathbf{x})|$. To evaluate the integrand in equation A-16, we use the approximation 16 from Ayzenberg et al. (2007).

To develop a similar expression for the PS-wavefield (equation A-9), we rewrite the terms involving G_S (see Ben-Menahem and Singh, 1998; their section 4.1 and Appendix A):

$$\nabla'\times\mathbf{G}_S = -\nabla\times\mathbf{G}_S = -\nabla\times\left\{\frac{1}{\rho^{(1)}\omega^2}\left[\frac{\omega^2}{[V_S^{(1)}]^2}g_S\mathbf{I} - \nabla g_S\nabla'\right]\right\}$$
$$= -\frac{1}{\rho^{(1)}[V_S^{(1)}]^2}\nabla\times(g_S\mathbf{I}) = -\frac{1}{\rho^{(1)}[V_S^{(1)}]^2}(\mathbf{I}\times\nabla g_S),$$

$$\rho^{(1)}[V_S^{(1)}]^2(\mathbf{n}'\times\mathbf{u}_{PS})\cdot(\nabla'\times\mathbf{G}_S) = -(\mathbf{n}'\times\mathbf{u}_{PS})\cdot(\mathbf{I}\times\nabla g_S)$$
$$= -[(\mathbf{n}'\times\mathbf{u}_{PS})\cdot\mathbf{I}]\times\nabla g_S = \nabla g_S\times(\mathbf{n}'\times\mathbf{u}_{PS})$$
$$= \nabla\times[g_S(\mathbf{n}'\times\mathbf{u}_{PS})], \tag{A-17}$$

and

$$\rho^{(1)}[V_S^{(1)}]^2((\nabla'\times\mathbf{u}_{PS})\times\mathbf{n}')\cdot\mathbf{G}_S$$
$$= \frac{[V_S^{(1)}]^2}{\omega^2}((\nabla'\times\mathbf{u}_{PS})\times\mathbf{n}')\cdot\left[\frac{\omega^2}{[V_S^{(1)}]^2}g_S\mathbf{I} - \nabla g_S\nabla'\right]$$
$$= \frac{[V_S^{(1)}]^2}{\omega^2}((\nabla'\times\mathbf{u}_{PS})\times\mathbf{n}')\cdot[-\nabla\cdot(\nabla g_S)\mathbf{I} + \nabla\nabla g_S]$$
$$= \frac{[V_S^{(1)}]^2}{\omega^2}\nabla\times[\nabla g_S\times((\nabla'\times\mathbf{u}_{PS})\times\mathbf{n}')]$$
$$= \frac{[V_S^{(1)}]^2}{\omega^2}\nabla\times\nabla\times[g_S((\nabla'\times\mathbf{u}_{PS})\times\mathbf{n}')]. \tag{A-18}$$

Substituting equations A-17 and A-18 into equation A-9, we find

$$\mathbf{u}_{\mathrm{PS}}(\mathbf{x}) = \nabla \times \int\int_{\mathrm{S}} g_{\mathrm{S}}(\mathbf{x}',\mathbf{x})\mathbf{n}' \times \mathbf{u}_{\mathrm{PS}}(\mathbf{x}')dS(\mathbf{x}') - \frac{[V_{\mathrm{S}}^{(1)}]^2}{\omega^2}\nabla \times \nabla \times \int\int_{\mathrm{S}} g_{\mathrm{S}}(\mathbf{x}',\mathbf{x})(\nabla' \times \mathbf{u}_{\mathrm{PS}}) \times \mathbf{n}'dS(\mathbf{x}'). \quad \text{(A-19)}$$

Next, we apply a series of vector identities to the term $g_{\mathrm{S}}(\mathbf{n}' \times \mathbf{u}_{\mathrm{PS}})$ (see Ben-Menahem and Singh, 1998; their Appendix A):

$$\begin{aligned} g_{\mathrm{S}}(\mathbf{n}' \times \mathbf{u}_{\mathrm{PS}}) &= -\frac{[V_{\mathrm{S}}^{(1)}]^2}{\omega^2}\nabla \cdot (\nabla g_{\mathrm{S}})(\mathbf{n}' \times \mathbf{u}_{\mathrm{PS}}) \\ &= -\frac{[V_{\mathrm{S}}^{(1)}]^2}{\omega^2}[\nabla \times ((\mathbf{n}' \times \mathbf{u}_{\mathrm{PS}}) \times \nabla g_{\mathrm{S}}) + (\mathbf{n}' \times \mathbf{u}_{\mathrm{PS}}) \cdot \nabla \nabla g_{\mathrm{S}}] \\ &= -\frac{[V_{\mathrm{S}}^{(1)}]^2}{\omega^2}[\nabla \times (\nabla' g_{\mathrm{S}} \times (\mathbf{n}' \times \mathbf{u}_{\mathrm{PS}})) + (\mathbf{n}' \times \mathbf{u}_{\mathrm{PS}}) \cdot \nabla \nabla g_{\mathrm{S}}] \\ &= -\frac{[V_{\mathrm{S}}^{(1)}]^2}{\omega^2}[\nabla \times (\mathbf{n}'(\mathbf{u}_{\mathrm{PS}} \cdot \nabla' g_{\mathrm{S}}) - \mathbf{u}_{\mathrm{PS}}(\mathbf{n}' \cdot \nabla' g_{\mathrm{S}})) + (\mathbf{n}' \times \mathbf{u}_{\mathrm{PS}}) \cdot \nabla \nabla g_{\mathrm{S}}] \\ &= \frac{[V_{\mathrm{S}}^{(1)}]^2}{\omega^2}\nabla \times [(\mathbf{n}' \cdot \nabla' g_{\mathrm{S}})\mathbf{u}_{\mathrm{PS}}] - \frac{[V_{\mathrm{S}}^{(1)}]^2}{\omega^2}[\nabla \times (\mathbf{n}'(\mathbf{u}_{\mathrm{PS}} \cdot \nabla' g_{\mathrm{S}})) + (\mathbf{n}' \times \mathbf{u}_{\mathrm{PS}}) \cdot \nabla \nabla g_{\mathrm{S}}]. \end{aligned} \quad \text{(A-20)}$$

Thus, equation A-19 can be rewritten as the sum of two surface integrals:

$$\mathbf{u}_{\mathrm{PS}}(\mathbf{x}) = -\frac{[V_{\mathrm{S}}^{(1)}]^2}{\omega^2}\nabla \times \nabla \times \int\int_{\mathrm{S}} \left[\frac{\partial g_{\mathrm{S}}(\mathbf{x}',\mathbf{x})}{\partial n'}\mathbf{u}_{\mathrm{PS}}(\mathbf{x}') - g_{\mathrm{S}}(\mathbf{x}',\mathbf{x})(\nabla' \times \mathbf{u}_{\mathrm{PS}}(\mathbf{x}')) \times \mathbf{n}(\mathbf{x}')\right] dS(\mathbf{x}') - \frac{[V_{\mathrm{S}}^{(1)}]^2}{\omega^2}\nabla \times \int\int_{\mathrm{S}} [\nabla (\mathbf{u}_{\mathrm{PS}}(\mathbf{x}') \cdot \nabla' g_{\mathrm{S}}(\mathbf{x}',\mathbf{x})) \times \mathbf{n}' + (\mathbf{n}' \times \mathbf{u}_{\mathrm{PS}}(\mathbf{x}')) \cdot \nabla \nabla g_{\mathrm{S}}(\mathbf{x}',\mathbf{x})]\, dS(\mathbf{x}'). \quad \text{(A-21)}$$

In the Fresnel-zone approximation, the second integral in equation A-21 is negligibly small compared with the first one. Taking into account equation A-4 and keeping only the first integral in equation A-21 yields

$$\mathbf{u}_{\mathrm{PS}}(\mathbf{x}) \simeq \int\int_{\mathrm{S}} \left[\frac{\partial g_{\mathrm{S}}(\mathbf{x}',\mathbf{x})}{\partial n'}\mathbf{u}_{\mathrm{PS}}(\mathbf{x}') - g_{\mathrm{S}}(\mathbf{x}',\mathbf{x})(\nabla' \times \mathbf{u}_{\mathrm{PS}}(\mathbf{x}')) \times \mathbf{n}(\mathbf{x}')\right] dS(\mathbf{x}'). \quad \text{(A-22)}$$

Expressing the reflected PS-wave at the interface through the corresponding ERC (equation F-6), we obtain the boundary values in equation A-22 as

$$\begin{aligned} \mathbf{u}_{\mathrm{PS}}(\mathbf{x}') &\simeq \chi_{\mathrm{PS}}(\mathbf{x}')[\mathbf{u}_{\mathrm{P}}^{\mathrm{inc}}(\mathbf{x}') \cdot \mathbf{h}_{\mathrm{P}}^{-}(\mathbf{x}')]\mathbf{h}_{\mathrm{S}}^{+}(\mathbf{x}'), \\ (\nabla' \times \mathbf{u}_{\mathrm{PS}}(\mathbf{x}')) \times \mathbf{n}(\mathbf{x}') &\simeq \chi_{\mathrm{PS}}(\mathbf{x}')\nabla' \times \{[\mathbf{u}_{\mathrm{P}}^{\mathrm{inc}}(\mathbf{x}') \cdot \mathbf{h}_{\mathrm{P}}^{-}(\mathbf{x}')]\mathbf{h}_{\mathrm{S}}^{+}(\mathbf{x}')\}. \end{aligned} \quad \text{(A-23)}$$

The PS reflected wavefield (equation A-22) can be evaluated using the elastic version of TWSM described for PP-waves in equations A-15 and A-16:

$$\mathbf{u}_{\mathrm{PS}}(\mathbf{x}) \simeq \sum_j \Delta\mathbf{B}_{\mathrm{PS}[j]}(\mathbf{x}), \quad \text{(A-24)}$$

where $\Delta\mathbf{B}_{\mathrm{PS}[j]}$ is the vector contribution of the surface element $\Delta\Pi_{[j]}$:

$$\Delta\mathbf{B}_{\mathrm{PS}[j]}(\mathbf{x}) = \int\int_{\Delta\Pi_{[j]}} \left[\frac{\partial g_{\mathrm{S}}(\mathbf{x}',\mathbf{x})}{\partial n'}\mathbf{u}_{\mathrm{PS}}(\mathbf{x}') - g_{\mathrm{S}}(\mathbf{x}',\mathbf{x})(\nabla' \times \mathbf{u}_{\mathrm{PS}}(\mathbf{x}')) \times \mathbf{n}(\mathbf{x}')\right] dS'. \quad \text{(A-25)}$$

The integrand in equation A-25 (as well as the one in the PP-wave equation A-16) is computed in the approximation by following the approach of Ayzenberg et al. (2007).

APPENDIX B

GENERALIZED PLANE WAVES

The conventional plane-wave decomposition of point-source radiation (the Weyl integral) can be used to obtain the reflected or transmitted wavefield for a plane interface between two homogeneous media. Here, we define generalized plane waves, which help extend the principle of plane-wave decomposition to interfaces of arbitrary shape and to account for local heterogeneity.

Consider wave propagation in a medium with a smooth curved interface S that separates two heterogeneous, arbitrarily anisotropic half-spaces $D^{(1)}$ and $D^{(2)}$. Each medium (superscript m) is described by the stiffness tensor $\mathbf{C}^{(m)}(\mathbf{x}) = [c_{ijkl}^{(m)}(\mathbf{x})]$ and density $\rho^{(m)}$; the unit vector $\mathbf{n}$ normal to the interface points toward $D^{(1)}$.

We define the curvilinear coordinates (s_1,s_2,s_3) in the immediate vicinity of the interface S inside $D^{(m)}$, such that (s_1,s_2) form the Chebychev coordinate mesh along the interface and the axis s_3 is normal to the interface and points inside $D^{(m)}$. Additionally, we define the local Cartesian coordinates (y_1,y_2,y_3) with the origin at point $\mathbf{x}'$. The axis y_3 coincides with s_3, whereas y_1 and y_2 are tangential to the curves s_1 and s_2 at $\mathbf{x}'$.

In the vicinity of point $\mathbf{x}'$, the Chebychev and local Cartesian coordinates are related as (Weatherburn, 1930; do Carmo, 1976; Klem-Musatov et al., 2004; Ayzenberg et al., 2007)

$$\begin{aligned} s_1(y_1,y_2,y_3) &= y_1 + O(y^3), \\ s_2(y_1,y_2,y_3) &= y_2 + O(y^3), \end{aligned}$$

$$s_3(y_1,y_2,y_3) = y_3 - \frac{1}{2}[C_1(\mathbf{x}')y_1^2 + C_2(\mathbf{x}')y_2^2] + O(y^3), \quad \text{(B-1)}$$

where $C_1(\mathbf{x}')$ and $C_2(\mathbf{x}')$ are the local curvatures of the interface along s_1 and s_2. The local and global Cartesian coordinates are related by the linear transform

$$y_i(x_1,x_2,x_3) = b_{ij}(\mathbf{x}')x_j, \quad \text{(B-2)}$$

where $b_{ij}(\mathbf{x}')$ are the elements of the linear transform matrix, which is specified, for example, in Červený (2001).

We introduce a generalized plane wave in the vicinity of the interface as

$$\mathbf{u}^{(m)}(s_1,s_2,s_3) = a^{(m)}\left[\mathbf{h}^{(m)} + i\mathbf{v}^{(m)}\frac{s_3^2}{2}\right]e^{i\omega(p_1s_1+p_2s_2+p_3s_3)}, \quad \text{(B-3)}$$

where p_1 and p_2 can be treated as the components of the slowness vector tangential to the interface. The normal slowness p_3, amplitude factor $a^{(m)}$, polarization vector $\mathbf{h}^{(m)}$ and its perturbation $\mathbf{v}^{(m)}$ must be found. At the interface where $s_3 = 0$ and the term proportional s_3^2 vanishes, equation B-3 describes a conventional plane wave (Červený, 2001).

The unknown parameters of the generalized plane wave can be determined by substituting equation B-3 for a point $\mathbf{x}'$ into the wave equation in the frequency domain (the stationary wave equation). First, we rewrite the stationary-wave equation in the two-index notation $\mathbf{C}_{jl}^{(m)}(\mathbf{x}') = [c_{ijkl}^{(m)}(\mathbf{x}')]$ (Kennett, 1994):

$$\mathbf{C}_{jl}^{(m)}(\mathbf{x}')\frac{\partial^2\mathbf{u}^{(m)}}{\partial x_j\partial x_l}(\mathbf{x}') + \frac{\partial\mathbf{C}_{jl}^{(m)}}{\partial x_j}(\mathbf{x}')\frac{\partial\mathbf{u}^{(m)}}{\partial x_l}(\mathbf{x}') + \rho\omega^2\mathbf{u}^{(m)}(\mathbf{x}') = 0. \quad \text{(B-4)}$$

Substituting the generalized plane wave (equation B-3) into equation B-4 and taking the coordinate transformations B-1 and B-2 into account yields

$$-\omega^2[\widetilde{\mathbf{C}}_{ik}^{(m)}(\mathbf{x}')p_ip_k - \rho^{(m)}\mathbf{I}]\mathbf{h}^{(m)} - i[\omega\mathbf{D}^{(m)}(\mathbf{x}')\mathbf{h}^{(m)} + \widetilde{\mathbf{C}}_{33}^{(m)}(\mathbf{x}')\mathbf{v}^{(m)}] = 0, \quad \text{(B-5)}$$

where $\widetilde{\mathbf{C}}_{ik}^{(m)}(\mathbf{x}') = b_{ij}(\mathbf{x}')b_{kl}(\mathbf{x}')\mathbf{C}_{jl}^{(m)}(\mathbf{x}')$ is the local stiffness tensor, and $\mathbf{D}^{(m)}(\mathbf{x}') = p_3[C_1(\mathbf{x}')\widetilde{\mathbf{C}}_{11}^{(m)}(\mathbf{x}') + C_2(\mathbf{x}')\widetilde{\mathbf{C}}_{22}^{(m)}(\mathbf{x}')] - p_l(\partial\widetilde{\mathbf{C}}_{jl}^{(m)}/\partial y_j)(\mathbf{x}')$ is the matrix that contains information about the local interface curvature. Both the real and imaginary parts of the left side of equation B-5 must go to zero. The real part of equation B-5 reduces to the well-known Christoffel equation (Červený, 2001):

$$[\widetilde{\mathbf{C}}_{ik}^{(m)}(\mathbf{x}')p_ip_k - \rho^{(m)}\mathbf{I}]\mathbf{h}^{(m)} = 0. \quad \text{(B-6)}$$

The slowness components $p_{Q3}^{(m)}(p_1,p_2;\mathbf{x}')$ of waves Q = P, S_1, and S_2 are obtained from the equation $\det[\widetilde{\mathbf{C}}_{ik}^{(m)}(\mathbf{x}')p_ip_k - \rho^{(m)}\mathbf{I}] = 0$. By substituting $p_{Q3}^{(m)}(p_1,p_2;\mathbf{x}')$ into equation B-6, we find the mutually orthogonal unit polarization vectors $\mathbf{h}_Q^{(m)}(\mathbf{x}')$. Note that the slownesses $p_{Q3}^{(m)}(p_1,p_2;\mathbf{x}')$ and polarization vectors $\mathbf{h}_Q^{(m)}(\mathbf{x}')$ are functions of the medium parameters at point $\mathbf{x}'$ but do not depend on the local interface curvature.

The imaginary part of equation B-5 constrains the perturbation vectors:

$$\mathbf{v}_Q^{(m)}(\mathbf{x}') = \omega[\widetilde{\mathbf{C}}_{33}^{(m)}(\mathbf{x}')]^{-1}\mathbf{D}^{(m)}(\mathbf{x}')\mathbf{h}_Q^{(m)}(\mathbf{x}'). \quad \text{(B-7)}$$

In the special case of a plane interface and homogeneous media, the derivatives $[\partial\widetilde{\mathbf{C}}_{jl}^{(m)}(\mathbf{x}')]/\partial y_j$ and curvatures $C_1(\mathbf{x}')$ and $C_2(\mathbf{x}')$ are equal to zero. Then the term $\mathbf{D}^{(m)}(\mathbf{x}')$ and the perturbation $\mathbf{v}_Q^{(m)}(\mathbf{x}')$ also vanish.

To solve the reflection/transmission problem, it is necessary to separate waves traveling toward the interface $[\mathbf{u}_Q^{(m)-}(s_1,s_2,s_3)]$ from those traveling away from it $[\mathbf{u}_Q^{(m)+}(s_1,s_2,s_3)]$ (Červený, 2001; Aki and Richards, 2002). We assume that sorting is done according to the orientation of the group velocity vector. If the slownesses $p_{Q3}^{(m)-}$ and $p_{Q3}^{(m)+}$ correspond to waves traveling toward and away from the interface, respectively, the generalized plane wave equation B-3 can be represented as

$$\mathbf{u}_Q^{(m)\pm}(s_1,s_2,s_3;\mathbf{x}') = a_Q^{(m)\pm}\left[\mathbf{h}_Q^{(m)\pm}(\mathbf{x}') + i\mathbf{v}_Q^{(m)\pm}(\mathbf{x}')\frac{s_3^2}{2}\right] \times e^{i\omega(p_1s_1+p_2s_2+p_{Q3}^{(m)\pm}(\mathbf{x}')s_3)}. \quad \text{(B-8)}$$

APPENDIX C

GENERALIZED PLANE-WAVE DECOMPOSITION AT THE INTERFACE

Here we introduce the generalized spectral integrals designed to decompose the displacement at the interface into the generalized plane P-, S_1-, and S_2-waves described in Appendix B. The total displacement inside $D^{(m)}$ can be expressed as the sum of the waves traveling toward and away from the interface (equation B-8):

$$\mathbf{u}^{(m)}(s_1,s_2,s_3) = \mathbf{u}^{(m)+}(s_1,s_2,s_3;\mathbf{x}') + \mathbf{u}^{(m)-}(s_1,s_2,s_3;\mathbf{x}'), \quad \text{(C-1)}$$

with the displacements represented by the generalized plane-wave decomposition

$$\mathbf{u}^{(m)\pm}(s_1,s_2,s_3;\mathbf{x}') = \frac{\omega^2}{2\pi}\int_{-\infty}^{+\infty}\int_{-\infty}^{+\infty}\left[\mathbf{H}^{(m)\pm} + i\mathbf{V}^{(m)\pm}\frac{s_3^2}{2}\right] \times \mathbf{E}^{(m)\pm}(s_3)\,\mathbf{a}^{(m)\pm}e^{i\omega(p_1s_1+p_2s_2)}\,dp_1dp_2. \quad \text{(C-2)}$$

Equation C-2 is a generalization of the conventional Weyl-type integral for curved interfaces and locally heterogeneous media. Whereas the Weyl decomposition is valid everywhere in the half-space $D^{(m)}$, the generalized expression C-2 is restricted to an infinitely thin layer covering the interface. Therefore, our formalism can be used to calculate the reflection response only in the immediate vicinity of the reflector.

The orthogonal polarization matrices $\mathbf{H}^{(m)\pm}$ are similar to those introduced by Červený (2001; his equation 5.4.110):

$$\mathbf{H}^{(m)\pm}(\mathbf{x}') = [\mathbf{h}_P^{(m)\pm}(\mathbf{x}')\,\mathbf{h}_{S1}^{(m)\pm}(\mathbf{x}')\,\mathbf{h}_{S_2}^{(m)\pm}(\mathbf{x}')],$$
$$\mathbf{V}^{(m)\pm}(\mathbf{x}') = [\mathbf{v}_P^{(m)\pm}(\mathbf{x}')\,\mathbf{v}_{S1}^{(m)\pm}(\mathbf{x}')\,\mathbf{v}_{S_2}^{(m)\pm}(\mathbf{x}')] \quad \text{(C-3)}$$

are the perturbation matrices and

$$\mathbf{E}^{(m)\pm}(s_3;\mathbf{x}') = \mathrm{diag}[e^{i\omega p_{\mathrm{P}3}^{(m)\pm}(\mathbf{x}')s_3}; e^{i\omega p_{\mathrm{S}_1,3}^{(m)\pm}(\mathbf{x}')s_3}; e^{i\omega p_{\mathrm{S}_2,3}^{(m)\pm}(\mathbf{x}')s_3}]. \quad \text{(C-4)}$$

The vectors $\mathbf{a}^{(m)\pm} = (a_{\mathrm{qP}}^{(m)\pm}, a_{\mathrm{qS}_1}^{(m)\pm}, a_{\mathrm{qS}_2}^{(m)\pm})^T$ contain the unknown amplitudes of the generalized plane waves.

The generalized plane-wave decomposition C-2 is valid for interfaces of arbitrary shape in heterogeneous anisotropic media. If the interface is plane, the curvatures $C_1(\mathbf{x}')$ and $C_2(\mathbf{x}')$ go to zero and the curvilinear coordinates (s_1,s_2,s_3) coincide with the local Cartesian coordinate system. If in addition the medium near the interface is homogeneous, the normal components of the slownesses and the polarization vectors do not depend on the reference point $\mathbf{x}'$. Then integral C-2 reduces to the well-known Weyl decomposition over conventional plane waves (Tsvankin, 1995, 2005; Červený, 2001; Aki and Richards, 2002).

At the interface ($s_3 \to 0$), equation C-2 reduces to the inverse Fourier integral,

$$\mathbf{u}^{(m)\pm}(s_1,s_2,0;\mathbf{x}') = \frac{\omega^2}{2\pi}\int_{-\infty}^{+\infty}\int_{-\infty}^{+\infty}\mathbf{H}^{(m)\pm}\mathbf{a}^{(m)\pm} \times e^{i\omega(p_1s_1+p_2s_2)}\,dp_1dp_2. \quad \text{(C-5)}$$

APPENDIX D

REFLECTION AND TRANSMISSION OPERATORS IN ANISOTROPIC MEDIA

The results of Appendix C make it possible to introduce the generalized plane-wave representation of the reflected wavefield at the interface. We assume that a point dislocation source is located in the upper half-space $D^{(1)}$ and that no sources exist in the lower half-space $D^{(2)}$. Then equations C-1 and C-5 can be written for $D^{(1)}$ as

$$\mathbf{u}^{(1)}(s_1,s_2,0) = \mathbf{u}^{(1)+}(s_1,s_2,0;\mathbf{x}') + \mathbf{u}^{(1)-}(s_1,s_2,0;\mathbf{x}'), \quad \text{(D-1)}$$

where $\mathbf{u}^{(1)-}(s_1,s_2,0;\mathbf{x}')$ and $\mathbf{u}^{(1)+}(s_1,s_2,0;\mathbf{x}')$ may be considered as the incident and reflected wavefields, respectively, at the interface. The reflected displacement $\mathbf{u}^{(1)+}(s_1,s_2,0;\mathbf{x}')$ is represented by the generalized spectral integral

$$\mathbf{u}^{(1)+}(s_1,s_2,0;\mathbf{x}') = \frac{\omega^2}{2\pi}\int_{-\infty}^{+\infty}\int_{-\infty}^{+\infty}\mathbf{H}^{(1)+}\mathbf{a}^{(1)+} \times e^{i\omega(p_1s_1+p_2s_2)}\,dp_1dp_2. \quad \text{(D-2)}$$

The amplitudes of the reflected $[\mathbf{a}^{(1)+}]$ and incident $[\mathbf{a}^{(1)-}]$ waves are related by the matrix $\mathbf{R}(p;\mathbf{x}')$ of the generalized plane-wave reflection and transmission coefficients:

$$\mathbf{a}^{(1)+} = \mathbf{R}(p;\mathbf{x}')\,\mathbf{a}^{(1)-}, \quad \text{(D-3)}$$

where $p = \sqrt{p_1^2 + p_2^2}$ and

$$\mathbf{R}(p;\mathbf{x}') = \begin{bmatrix} R_{\mathrm{PP}} & R_{\mathrm{S}_1\mathrm{P}} & R_{\mathrm{S}_2\mathrm{P}} \\ R_{\mathrm{PS}_1} & R_{\mathrm{S}_1\mathrm{S}_1} & R_{\mathrm{S}_2\mathrm{S}_1} \\ R_{\mathrm{PS}_2} & R_{\mathrm{S}_1\mathrm{S}_2} & R_{\mathrm{S}_2\mathrm{S}_2} \end{bmatrix}. \quad \text{(D-4)}$$

The matrix D-4 coincides with the one introduced by Červený (2001) if the stiffness coefficients are fixed at location $\mathbf{x}'$ and the plane interface is tangential to the actual reflector at $\mathbf{x}'$.

Because the matrix $\mathbf{H}^{(1)-}$ is orthogonal, it satisfies the equality $[\mathbf{H}^{(1)-}]^{-1} = [\mathbf{H}^{(1)-}]^T$. From equation C-5, it follows that $\mathbf{u}^{(1)-}(p_1,p_2,0;\mathbf{x}') = \mathbf{H}^{(1)-}\mathbf{a}^{(1)-}$, which allows us to obtain the amplitude vector of the incident wave in the form

$$\mathbf{a}^{(1)-} = [\mathbf{H}^{(1)-}]^T\,\mathbf{u}^{(1)-}(p_1,p_2,0;\mathbf{x}'). \quad \text{(D-5)}$$

Taking into account equations D-3 and D-5, the reflected wavefield (equation D-2) can be represented as

$$\mathbf{u}^{(1)+}(s_1,s_2,0;\mathbf{x}') = \frac{\omega^2}{2\pi}\int_{-\infty}^{+\infty}\int_{-\infty}^{+\infty}\mathbf{H}^{(1)+}\mathbf{R}(p;\mathbf{x}')[\mathbf{H}^{(1)-}]^T \cdot\mathbf{u}^{(1)-}(p_1,p_2,0;\mathbf{x}') \cdot e^{i\omega(p_1s_1+p_2s_2)}\,dp_1dp_2, \quad \text{(D-6)}$$

where the spatial spectrum of the incident wavefield is expressed by the generalized Fourier integral over the curved interface:

$$\mathbf{u}^{(1)-}(p_1,p_2,0;\mathbf{x}') = \frac{1}{2\pi}\int_{-\infty}^{+\infty}\int_{-\infty}^{+\infty}\mathbf{u}^{(1)-}(s_1,s_2,0;\mathbf{x}') \times e^{-i\omega(p_1s_1+p_2s_2)}ds_1ds_2. \quad \text{(D-7)}$$

For the incident spherical P-wave excited by a point source, $\mathbf{u}^{(1)-}(s_1,s_2,0;\mathbf{x}') = \mathbf{u}_P^{(1)-}(s_1,s_2,0;\mathbf{x}')$. The polarization matrix $\mathbf{H}^{(1)+}$ can be separated into the matrices for P- and S-waves:

$$\mathbf{H}^{(1)+}(\mathbf{x}') = \mathbf{H}_{\mathrm{P}}^{(1)+}(\mathbf{x}') + \mathbf{H}_{\mathrm{S}}^{(1)+}(\mathbf{x}') \quad \text{(D-8)}$$

and

$$\mathbf{H}_{\mathrm{P}}^{(1)+}(\mathbf{x}') = [\mathbf{h}_{\mathrm{P}}^{(m)\pm}(\mathbf{x}') \quad 0 \quad 0],$$

$$\mathbf{H}_{\mathrm{S}}^{(1)+}(\mathbf{x}') = [0 \quad \mathbf{h}_{\mathrm{S}_1}^{(m)\pm}(\mathbf{x}') \quad \mathbf{h}_{\mathrm{S}_2}^{(m)\pm}(\mathbf{x}')]. \quad \text{(D-9)}$$

The reflected wavefield (equation D-6) can be decomposed into the displacements of PP-waves and split PS-waves. The spectral representation for PP-waves (Q = P) or converted PQ-waves (Q = S_1 or S_2) at the interface is given by

$$\mathbf{u}_{\mathrm{PQ}}^{(1)+}(s_1,s_2,0;\mathbf{x}') = \frac{\omega^2}{2\pi}\int_{-\infty}^{+\infty}\int_{-\infty}^{+\infty}\mathbf{H}_{\mathrm{Q}}^{(1)+}\mathbf{R}(p;\mathbf{x}')[\mathbf{H}^{(1)-}]^T \cdot\mathbf{u}_{\mathrm{P}}^{(1)-}(p_1,p_2,0;\mathbf{x}') \times e^{i\omega(p_1s_1+p_2s_2)}\,dp_1dp_2. \quad \text{(D-10)}$$

The displacement component orthogonal to the interface is

$$u^{(1)+}_{\mathrm{PQ,norm}}(s_1,s_2,0;\mathbf{x}') = \frac{\omega^2}{2\pi}\int_{-\infty}^{+\infty}\int_{-\infty}^{+\infty} R_{\mathrm{PQ}}(p;\mathbf{x}')\frac{h^{(1)+}_{\mathrm{Q,norm}}(\mathbf{x}')}{h^{(1)-}_{\mathrm{P,norm}}(\mathbf{x}')} \times u^{(1)-}_{\mathrm{P,norm}}(p_1,p_2,0;\mathbf{x}') \times e^{i\omega(p_1s_1+p_2s_2)}\,dp_1dp_2. \quad \text{(D-11)}$$

For the two displacement components ($j = 1,2$) tangential to the interface, we have

$$u^{(1)+}_{\mathrm{PQ},j}(s_1,s_2,0;\mathbf{x}') = \frac{\omega^2}{2\pi}\int_{-\infty}^{+\infty}\int_{-\infty}^{+\infty} R_{\mathrm{PQ}}(p;\mathbf{x}')\frac{h^{(1)+}_{\mathrm{Q},j}(\mathbf{x}')}{h^{(1)-}_{\mathrm{P},j}(\mathbf{x}')} \times u^{(1)-}_{\mathrm{P},j}(p_1,p_2,0;\mathbf{x}')e^{i\omega(p_1s_1+p_2s_2)}\,dp_1dp_2. \quad \text{(D-12)}$$

APPENDIX E

PLANE-WAVE REFLECTION COEFFICIENTS FOR VTI MEDIA

Here, we reproduce the derivation of the amplitude-normalized PWRC in our notation and correct typos in the published solutions.

The symmetry axis of the reflecting TI medium in our model is assumed to be orthogonal to the interface. Therefore, the PWRCs in equations D-10–D-12 coincide with those for a horizontal interface between isotropic and VTI media. Also, for purposes of computing the reflection coefficient, the slowness vectors of the incident, reflected, and transmitted waves can be confined to the (x_1, x_3) plane. The vertical slowness components $q^{(m)}$ are obtained from the eigenvalues of the Christoffel equation:

$$\det\begin{pmatrix} c^{(m)}_{11}p^2 + c^{(m)}_{55}(q^{(m)})^2 - \rho^{(m)} & (c^{(m)}_{13}+c^{(m)}_{55})pq^{(m)} \\ (c^{(m)}_{13}+c^{(m)}_{55})pq^{(m)} & c^{(m)}_{33}(q^{(m)})^2 + c^{(m)}_{55}p^2 - \rho^{(m)} \end{pmatrix} = 0. \quad \text{(E-1)}$$

The vertical slownesses of P- and SV-waves are given by

$$q^{(m)}_{\mathrm{P}} = \frac{1}{\sqrt{2}}\sqrt{K^{(m)}_1 - \sqrt{K^{(m)2}_1 - 4K^{(m)}_2K^{(m)}_3}},$$

$$q^{(m)}_{\mathrm{S}} = \frac{1}{\sqrt{2}}\sqrt{K^{(m)}_1 + \sqrt{K^{(m)2}_1 - 4K^{(m)}_2K^{(m)}_3}}, \quad \text{(E-2)}$$

where

$$K^{(m)}_1 = \frac{\rho^{(m)}}{c^{(m)}_{33}} + \frac{\rho^{(m)}}{c^{(m)}_{55}} - \left(\frac{c^{(m)}_{11}}{c^{(m)}_{55}} + \frac{c^{(m)}_{55}}{c^{(m)}_{33}} - \frac{(c^{(m)}_{13}+c^{(m)}_{55})^2}{c^{(m)}_{33}c^{(m)}_{55}}\right)p^2,$$

$$K^{(m)}_2 = \frac{c^{(m)}_{11}}{c^{(m)}_{33}}p^2 - \frac{\rho^{(m)}}{c^{(m)}_{33}},$$

$$K^{(m)}_3 = p^2 - \frac{\rho^{(m)}}{c^{(m)}_{33}}. \quad \text{(E-3)}$$

The eigenvectors of the Christoffel equation E-1 yield the directional cosines of the polarization vectors:

$$l^{(m)}_{\mathrm{P}} = \sqrt{\frac{c^{(m)}_{33}q^{(m)2}_{\mathrm{P}} + c^{(m)}_{55}p^2 - \rho^{(m)}}{(c^{(m)}_{33}+c^{(m)}_{55})q^{(m)2}_{\mathrm{P}} + (c^{(m)}_{11}+c^{(m)}_{55})p^2 - 2\rho^{(m)}}},$$

$$m^{(m)}_{\mathrm{P}} = \sqrt{\frac{c^{(m)}_{55}q^{(m)2}_{\mathrm{P}} + c^{(m)}_{11}p^2 - \rho^{(m)}}{(c^{(m)}_{33}+c^{(m)}_{55})q^{(m)2}_{\mathrm{P}} + (c^{(m)}_{11}+c^{(m)}_{55})p^2 - 2\rho^{(m)}}},$$

$$l^{(m)}_{\mathrm{S}} = \sqrt{\frac{c^{(m)}_{55}q^{(m)2}_{\mathrm{S}} + c^{(m)}_{11}p^2 - \rho^{(m)}}{(c^{(m)}_{33}+c^{(m)}_{55})q^{(m)2}_{\mathrm{S}} + (c^{(m)}_{11}+c^{(m)}_{55})p^2 - 2\rho^{(m)}}},$$

$$m^{(m)}_{\mathrm{S}} = \sqrt{\frac{c^{(m)}_{33}q^{(m)2}_{\mathrm{S}} + c^{(m)}_{55}p^2 - \rho^{(m)}}{(c^{(m)}_{33}+c^{(m)}_{55})q^{(m)2}_{\mathrm{S}} + (c^{(m)}_{11}+c^{(m)}_{55})p^2 - 2\rho^{(m)}}}. \quad \text{(E-4)}$$

Next, we introduce a 4×4 matrix with the following elements:

$$\begin{aligned}
&m_{11} = l^{(1)}_{\mathrm{P}}, \quad m_{12} = m^{(1)}_{\mathrm{S}}, \quad m_{13} = -l^{(2)}_{\mathrm{P}}, \quad m_{14} = -m^{(2)}_{\mathrm{S}},\\
&m_{31} = m^{(1)}_{\mathrm{P}}, \quad m_{32} = -l^{(1)}_{\mathrm{S}}, \quad m_{33} = m^{(2)}_{\mathrm{P}}, \quad m_{34} = -l^{(2)}_{\mathrm{S}},\\
&m_{21} = pl^{(1)}_{\mathrm{P}}c^{(1)}_{13} + q^{(1)}_{\mathrm{P}}m^{(1)}_{\mathrm{P}}c^{(1)}_{33},\\
&m_{22} = pm^{(1)}_{\mathrm{S}}c^{(1)}_{13} - q^{(1)}_{\mathrm{S}}l^{(1)}_{\mathrm{S}}c^{(1)}_{33},\\
&m_{23} = -pl^{(2)}_{\mathrm{P}}c^{(2)}_{13} - q^{(2)}_{\mathrm{P}}m^{(2)}_{\mathrm{P}}c^{(2)}_{33},\\
&m_{24} = pm^{(2)}_{\mathrm{S}}c^{(2)}_{13} - q^{(2)}_{\mathrm{S}}l^{(2)}_{\mathrm{S}}c^{(2)}_{33},\\
&m_{41} = pm^{(1)}_{\mathrm{P}}c^{(1)}_{55} + q^{(1)}_{\mathrm{P}}l^{(1)}_{\mathrm{P}}c^{(1)}_{55},\\
&m_{42} = -pl^{(1)}_{\mathrm{S}}c^{(1)}_{55} + q^{(1)}_{\mathrm{S}}m^{(1)}_{\mathrm{S}}c^{(1)}_{55},\\
&m_{43} = pm^{(2)}_{\mathrm{P}}c^{(2)}_{55} + q^{(2)}_{\mathrm{P}}l^{(2)}_{\mathrm{P}}c^{(2)}_{55},\\
&m_{44} = -pl^{(2)}_{\mathrm{S}}c^{(2)}_{55} + q^{(2)}_{\mathrm{S}}m^{(2)}_{\mathrm{S}}c^{(2)}_{55}.
\end{aligned} \quad \text{(E-5)}$$

(Note the misprint in the equivalent definition of the elements m_{ij} in Rüger [2002, p. 51–52]. In his notation, the normalized stiffnesses a_{ij} should be replaced with c_{ij}.)

The cofactors of the matrix m_{ij} are

$$\begin{aligned}
M_{11} &= m_{22}(m_{33}m_{44} - m_{34}m_{43}) - m_{23}(m_{32}m_{44} - m_{34}m_{42}) + m_{24}(m_{32}m_{43} - m_{33}m_{42}),\\
M_{21} &= -m_{12}(m_{33}m_{44} - m_{34}m_{43}) + m_{13}(m_{32}m_{44} - m_{34}m_{42}) - m_{14}(m_{32}m_{43} - m_{33}m_{42}),\\
M_{31} &= m_{12}(m_{23}m_{44} - m_{24}m_{43}) - m_{13}(m_{22}m_{44} - m_{24}m_{42}) + m_{14}(m_{22}m_{43} - m_{23}m_{42}),\\
M_{41} &= -m_{12}(m_{23}m_{34} - m_{24}m_{33}) + m_{13}(m_{22}m_{34} - m_{24}m_{32}) - m_{14}(m_{22}m_{33} - m_{23}m_{32}),\\
M_{12} &= -m_{21}(m_{33}m_{44} - m_{34}m_{43}) + m_{23}(m_{31}m_{44} - m_{34}m_{41}) - m_{24}(m_{31}m_{43} - m_{33}m_{41}),\\
M_{22} &= m_{11}(m_{33}m_{44} - m_{34}m_{43}) - m_{13}(m_{31}m_{44} - m_{34}m_{41}) + m_{14}(m_{31}m_{43} - m_{33}m_{41}),\\
M_{32} &= -m_{11}(m_{23}m_{44} - m_{24}m_{43}) + m_{13}(m_{21}m_{44} - m_{24}m_{41}) - m_{14}(m_{21}m_{43} - m_{23}m_{41}),
\end{aligned}$$

$$M_{42} = m_{11}(m_{23}m_{34} - m_{24}m_{33}) - m_{13}(m_{21}m_{34} - m_{24}m_{31}) + m_{14}(m_{21}m_{33} - m_{23}m_{31}). \quad \text{(E-6)}$$

Then the plane-wave reflection coefficients $R_{PP}(p)$ and $R_{PS}(p)$ can be found as

$$R_{PP}(p) = \frac{-m_{11}M_{11} - m_{21}M_{21} + m_{31}M_{31} + m_{41}M_{41}}{m_{11}M_{11} + m_{12}M_{12} + m_{13}M_{13} + m_{14}M_{14}} \quad \text{(E-7)}$$

and

$$R_{PS}(p) = \frac{-m_{11}M_{12} - m_{21}M_{22} + m_{31}M_{32} + m_{41}M_{42}}{m_{11}M_{11} + m_{12}M_{12} + m_{13}M_{13} + m_{14}M_{14}}. \quad \text{(E-8)}$$

APPENDIX F

EFFECTIVE REFLECTION COEFFICIENTS FOR CURVED INTERFACES

For arbitrary interface geometry and heterogeneity, evaluation of integral 7 is complicated because it involves generating the curvilinear mesh (s_1,s_2) and applying it in the computation of the spectrum $\mathbf{u}_P^{(1)-}(p_1,p_2,0;\mathbf{x}')$ by means of the Fourier transform 8. However, the integration in equation 7 is performed over the tangential slowness plane (p_1,p_2) and is not explicitly related to the geometry of the mesh (s_1,s_2). This fact can be used to represent these integrals in the form similar to equation 6:

$$\mathbf{u}_{PQ}(\mathbf{x}') = [\chi_{PQ}(\mathbf{x}')\,\mathbf{h}_Q^+(\mathbf{x}') + \varepsilon_{PQ}(\mathbf{x}')\,\mathbf{e}_Q(\mathbf{x}')]\,[\mathbf{u}_P^{inc}(\mathbf{x}')\cdot\mathbf{h}_P^-(\mathbf{x}')], \quad \text{(F-1)}$$

where $\chi_{PQ}(\mathbf{x}')$ are the ERCs, $\varepsilon_{PQ}(\mathbf{x}')$ are the spurious reflection coefficients, and $\mathbf{e}_Q(\mathbf{x}')$ are the unit vectors orthogonal to the polarization vectors $\mathbf{h}_Q^+(\mathbf{x}')$. We define the effective and spurious reflection coefficients as

$$\chi_{PQ}(\mathbf{x}') = \frac{\mathbf{u}_{PQ}(\mathbf{x}')\cdot\mathbf{h}_Q^+(\mathbf{x}')}{\mathbf{u}_P^{inc}(\mathbf{x}')\cdot\mathbf{h}_P^-(\mathbf{x}')} \quad \text{(F-2)}$$

and

$$\varepsilon_{PQ}(\mathbf{x}') = \frac{\mathbf{u}_{PQ}(\mathbf{x}')\cdot\mathbf{e}_Q(\mathbf{x}')}{\mathbf{u}_P^{inc}(\mathbf{x}')\cdot\mathbf{h}_P^-(\mathbf{x}')}. \quad \text{(F-3)}$$

The ERC in equation F-2 is expressed through the projection of the displacement of the reflected PQ-mode onto the polarization vector of the corresponding plane wave. Therefore, ERCs generalize PWRCs for point sources and curved interfaces. In the seismic frequency range, ERCs describe the main component of the reflected wavefield. Spurious reflection coefficients represent diffraction corrections, which are much smaller in magnitude and can be neglected in equation F-1.

For acoustic wave propagation, integrals similar to those in equations D-11 and D-12 can be computed approximately in the dominant-frequency approximation for an apparent source location and a plane interface tangential to the actual reflector at point $\mathbf{x}'$ (Ayzenberg et al., 2007). Then the problem reduces to the evaluation of Fourier-Bessel integrals similar to the ones for a plane interface. The same approach can be applied to elastic media because it is based entirely on the geometry of the incident P-wave. The incidence angle $\theta(\mathbf{x}')$ stays the same and the actual source moves along the ray to a new position at distance $R^*(\mathbf{x}')$ from the plane interface:

$$R^*(\mathbf{x}') = R(\mathbf{x}')\frac{2 - \sin^2\theta(\mathbf{x}')}{2 - \sin^2\theta(\mathbf{x}') - 2R(\mathbf{x}')H(\mathbf{x}')\cos\theta(\mathbf{x}')}, \quad \text{(F-4)}$$

where $H(\mathbf{x}')$ is the mean curvature of the interface. If the reflector is locally plane and $H(\mathbf{x}') = 0$, the distance $R^*(\mathbf{x}')$ reduces to $R(\mathbf{x}')$.

Adapting the results by Ayzenberg et al. (2007) for scalar integrals similar to integral 7, we replace the actual incident P-wave $\mathbf{u}_P^{inc}(s_1,s_2,0;\mathbf{x}')$ in equation 8 with an apparent spherical wave $\mathbf{u}_P^*(s_1,s_2,0;\mathbf{x}')$ and assume that the mesh (s_1,s_2) belongs to the plane tangential to the actual reflector at point $\mathbf{x}'$. Then the ERC in equation F-2 becomes

$$\chi_{PQ}(\mathbf{x}') \simeq \chi_{PQ}(\theta(\mathbf{x}'),L(\mathbf{x}')) = \frac{\mathbf{u}_{PQ}^*(\mathbf{x}')\cdot\mathbf{h}_Q^+(\mathbf{x}')}{\mathbf{u}_P^*(\mathbf{x}')\cdot\mathbf{h}_P^-(\mathbf{x}')}, \quad \text{(F-5)}$$

where $L(\mathbf{x}') = \omega R^*(\mathbf{x}')/V_P^{(1)}$ is a dimensionless frequency-dependent parameter. Unlike integral 8, equation F-5 does not involve integration over the curvilinear mesh. For each point $\mathbf{x}'$ at the curved reflector, the displacement $\mathbf{u}_{PQ}^*(\mathbf{x}')$ is given by the conventional Weyl-type integral, whereas $\mathbf{u}_P^*(\mathbf{x}')$ describes the apparent incident P-wave in the plane tangential to the reflector at point $\mathbf{x}'$.

Neglecting the term containing $\varepsilon_{PQ}(\mathbf{x}')$, we rewrite equation F-1 as

$$\mathbf{u}_{PQ}(\mathbf{x}') \simeq \chi_{PQ}(\theta(\mathbf{x}'),L(\mathbf{x}'))\,[\mathbf{u}_P^{inc}(\mathbf{x}')\cdot\mathbf{h}_P^-(\mathbf{x}')]\,\mathbf{h}_Q^+(\mathbf{x}'). \quad \text{(F-6)}$$

The apparent incident P-wave is described by

$$\mathbf{u}_P^*(s_1,s_2,s_3;\mathbf{x}') = \text{grad}\,\frac{e^{ik_PR^*}}{R^*} = \left(ik_P - \frac{1}{R^*}\right)\frac{e^{ik_PR^*}}{R^*}\left(\frac{x_1^{S*} - s_1}{R^*}, \frac{x_2^{S*} - s_2}{R^*}, \frac{x_3^{S*} - s_3}{R^*}\right)^T, \quad \text{(F-7)}$$

where $\mathbf{x}^{S*} = (x_1^{S*},x_2^{S*},x_3^{S*})$ are the apparent source coordinates in the global Cartesian system, $R^* = \sqrt{l^2 + r^2}$, $l = |x_3^{S*} - s_3|$, and $r = \sqrt{(x_1^{S*} - s_1)^2 + (x_2^{S*} - s_2)^2}$. Hereafter, (s_1,s_2) are the local Cartesian coordinates in the plane tangential to the actual reflector at point $\mathbf{x}'$. Note that the product $\mathbf{u}_P^*(\mathbf{x}')\cdot\mathbf{h}_P^-(\mathbf{x}')$ from equation F-5 is

$$\mathbf{u}_P^*(s_1,s_2,s_3;\mathbf{x}')\cdot\mathbf{h}_P^-(\mathbf{x}') = \left(ik_P - \frac{1}{R^*}\right)\frac{e^{ik_PR^*}}{R^*}. \quad \text{(F-8)}$$

The plane-wave decomposition of the displacement of the apparent incident P-wave has the form (Aki and Richards, 2002)

$$\mathbf{u}_{\mathrm{P}}^{*}(s_1,s_2,s_3;\mathbf{x}') = \mathrm{grad}\left[\frac{\omega}{2\pi}\int_{-\infty}^{+\infty}\int_{-\infty}^{+\infty}\frac{ie^{i\omega l p_{\mathrm{P3}}^{(1)}}}{p_{\mathrm{P3}}^{(1)}} \times e^{i\omega(p_1 s_1 + p_2 s_2)}\,dp_1 dp_2\right]. \quad \text{(F-9)}$$

Interchanging the order of differentiation and integration and setting $s_3 = 0$, we obtain

$$\mathbf{u}_{\mathrm{P}}^{*}(p_1,p_2,0;\mathbf{x}') = -\omega\frac{e^{i\omega l p_{\mathrm{P3}}^{(1)}}}{p_{\mathrm{P3}}^{(1)}}(p_1,p_2,-p_{\mathrm{P3}}^{(1)})^T. \quad \text{(F-10)}$$

Thus, the unit polarization vectors of the incident P-wave ($\mathbf{h}_{\mathrm{P}}^{(1)-}$) and reflected PP-wave ($\mathbf{h}_{\mathrm{P}}^{(1)+}$) are given by

$$\begin{aligned}\mathbf{h}_{\mathrm{P}}^{(1)-} &= V_{\mathrm{P}}^{(1)}(p_1,p_2,-p_{\mathrm{P3}}^{(1)})^T = V_{\mathrm{P}}^{(1)}(p\cos\psi, p\sin\psi,\\ &\quad -p_{\mathrm{P3}}^{(1)})^T,\\ \mathbf{h}_{\mathrm{P}}^{(1)+} &= V_{\mathrm{P}}^{(1)}(p\cos\psi, p\sin\psi, p_{\mathrm{P3}}^{(1)})^T, \end{aligned} \quad \text{(F-11)}$$

where ψ is the polar angle in the plane (p_1,p_2). It is straightforward to show that the polarization of the converted PS-wave is

$$\mathbf{h}_{\mathrm{S}}^{(1)+} = V_{\mathrm{S}}^{(1)}(p_{\mathrm{S3}}^{(1)}\cos\psi, p_{\mathrm{S3}}^{(1)}\sin\psi, -p)^T. \quad \text{(F-12)}$$

Hence, for the PP-wave, $h_{\mathrm{P,norm}}^{+}/h_{\mathrm{P,norm}}^{-} = -1$ and $h_{\mathrm{P,tan}}^{+}/h_{\mathrm{P,tan}}^{-} = 1$. For the PS-wave, $h_{\mathrm{S,norm}}^{+}/h_{\mathrm{P,norm}}^{-} = (V_{\mathrm{S}}^{(1)}p)/(V_{\mathrm{P}}^{(1)}p_{\mathrm{P3}}^{(1)})$ and $h_{\mathrm{S,tan}}^{+}/h_{\mathrm{P,tan}}^{-} = (V_{\mathrm{S}}^{(1)}p_{S3}^{(1)})/(V_{\mathrm{P}}^{(1)}p)$.

Using equations F-7 and 7, we find the normal to the interface component of the displacement vector of the reflected PQ-mode:

$$u_{\mathrm{PQ,norm}}^{*}(s_1,s_2,0;\mathbf{x}') = \frac{\omega^2}{2\pi}\int_{-\infty}^{+\infty}\int_{-\infty}^{+\infty}R_{\mathrm{PQ}}(p;\mathbf{x}')\frac{h_{\mathrm{Q,norm}}^{(1)+}(\mathbf{x}')}{h_{\mathrm{P,norm}}^{(1)-}(\mathbf{x}')} \times e^{i\omega l p_{\mathrm{P3}}^{(1)}}e^{i\omega(p_1 s_1 + p_2 s_2)}\,dp_1 dp_2. \quad \text{(F-13)}$$

In the polar coordinates (p,ψ) and (r,φ), equation F-13 reduces to the Fourier-Bessel integral:

$$u_{\mathrm{PQ,norm}}^{*}(s_1,s_2,0;\mathbf{x}') = \omega^2\int_{0}^{+\infty}R_{\mathrm{PQ}}(p;\mathbf{x}'')\frac{h_{\mathrm{Q,norm}}^{(1)+}(\mathbf{x}')}{h_{\mathrm{P,norm}}^{(1)-}(\mathbf{x}')} \times e^{i\omega l p_{\mathrm{P3}}^{(1)}}J_0(r\omega p)\,pdp, \quad \text{(F-14)}$$

where J_0 is the zero-order Bessel function:

$$J_0(r\omega p) = \frac{1}{2\pi}\int_0^{2\pi}e^{ir\omega p\cos(\psi-\varphi)}d\psi. \quad \text{(F-15)}$$

As follows from equation 7, the two tangential displacement components of the reflected PQ-wave are

$$u_{\mathrm{PQ},j}^{*}(s_1,s_2,0;\mathbf{x}') = -\frac{\omega^2}{2\pi}\int_{-\infty}^{+\infty}\int_{-\infty}^{+\infty}R_{\mathrm{PQ}}(p;\mathbf{x}')\frac{h_{\mathrm{Q},j}^{(1)+}(\mathbf{x}')}{h_{\mathrm{P},j}^{(1)-}(\mathbf{x}')} \times\frac{e^{i\omega l p_{\mathrm{P3}}^{(1)}}}{p_{\mathrm{P3}}^{(1)}}p_j e^{i\omega(p_1 s_1 + p_2 s_2)}\,dp_1 dp_2. \quad \text{(F-16)}$$

In the polar coordinates (r,φ),

$$\begin{aligned}u_{\mathrm{PQ,tan}}^{*}(\mathbf{x}') &= u_{\mathrm{PQ},1}^{*}(\mathbf{x}')\cos\varphi + u_{\mathrm{PQ},2}^{*}(\mathbf{x}')\sin\varphi,\\ u_{\mathrm{PQ,tan}}^{*}(s_1,s_2,0;\mathbf{x}') &= -\frac{\omega^2}{2\pi}\int_{-\infty}^{+\infty}\int_{-\infty}^{+\infty}R_{\mathrm{PQ}}(p;\mathbf{x}')\frac{h_{\mathrm{Q},j}^{(1)+}(\mathbf{x}')}{h_{\mathrm{P},j}^{(1)-}(\mathbf{x}')} \times\frac{e^{i\omega l p_{\mathrm{P3}}^{(1)}}}{p_{\mathrm{P3}}^{(1)}}p\cos(\psi-\varphi) \times e^{i\omega(p_1 s_1 + p_2 s_2)}dp_1 dp_2. \end{aligned} \quad \text{(F-17)}$$

Equation F-17 can also be reduced to the Fourier-Bessel integral:

$$u_{\mathrm{PQ,tan}}^{*}(s_1,s_2,0;\mathbf{x}') = -\omega^2\int_{0}^{+\infty}R_{\mathrm{PQ}}(p;\mathbf{x}')\frac{h_{\mathrm{Q},j}^{(1)+}(\mathbf{x}')}{h_{\mathrm{P},j}^{(1)-}(\mathbf{x}')}\frac{ie^{i\omega l p_{\mathrm{P3}}^{(1)}}}{p_{\mathrm{P3}}^{(1)}} \times J_1(r\omega p)p^2 dp, \quad \text{(F-18)}$$

where J_1 is the first-order Bessel function:

$$J_1(r\omega p) = -\frac{i}{2\pi}\int_0^{2\pi}\cos(\psi-\varphi)e^{ir\omega p\cos(\psi-\varphi)}d\psi. \quad \text{(F-19)}$$

The normal and tangential to the reflector components of the polarization vectors can be written as $h_{\mathrm{P,norm}}^{(1)+} = \cos\theta(\mathbf{x}')$, $h_{\mathrm{P,tan}}^{(1)+} = \sin\theta(\mathbf{x}')$, and $h_{\mathrm{S,norm}}^{(1)+} = -\sin\theta_S(\mathbf{x}')$, and $h_{\mathrm{S,tan}}^{(1)+} = \cos\theta_S\mathbf{x}'$, where $\theta(\mathbf{x}')$ is the P-wave incidence angle and $\theta_S(\mathbf{x}')$ is the S-wave reflection angle determined from Snell's law as $\theta_{\mathrm{S}}(\mathbf{x}') = \sin^{-1}[V_{\mathrm{S}}^{(1)}/V_{\mathrm{P}}^{(1)}\sin\theta(\mathbf{x}')]$.

Finally, substituting the Fourier-Bessel integrals F-14 and F-18 and the polarization components into the definition F-5 of the ERC yields

$$\begin{aligned}&\chi_{\mathrm{PP}}(\theta(\mathbf{x}'),L(\mathbf{x}'))\\ &\quad = \frac{u_{\mathrm{PP,norm}}^{*}(\mathbf{x}')\cos\theta(\mathbf{x}') + u_{\mathrm{PP,tan}}^{*}(\mathbf{x}')\sin\theta(\mathbf{x}')}{\left(ik_{\mathrm{P}} - \frac{1}{R^*}\right)\frac{e^{ik_{\mathrm{P}}R^*}}{R^*}},\\ &\chi_{\mathrm{PS}}(\theta(\mathbf{x}'),L(\mathbf{x}'))\\ &\quad = \frac{-u_{\mathrm{PS,norm}}^{*}(\mathbf{x}')\sin\theta_{\mathrm{S}}(\mathbf{x}') + u_{\mathrm{PS,tan}}^{*}(\mathbf{x}')\cos\theta_{\mathrm{S}}(\mathbf{x}')}{\left(ik_{\mathrm{P}} - \frac{1}{R^*}\right)\frac{e^{ik_{\mathrm{P}}R^*}}{R^*}}. \end{aligned} \quad \text{(F-20)}$$

REFERENCES

Aizenberg, A. M., 1992, A self-similar conformal analog of wave equation in 3D nonhomogeneous space: Russian Geology and Geophysics, **33**, 116–121.

———, 1993a, Special function of eddy diffusion equation in 3D inhomogeneous space: Russian Geology and Geophysics, **34**, 107–114.

———, 1993b, A system of irregular fundamental solutions to wave equation in a three-dimensional inhomogeneous medium: Russian Geology and Geophysics, **34**, 105–113.

Aki, K., and P. G. Richards, 2002, Quantitative seismology: University Science Books.

Ayzenberg, M. A., A. M. Aizenberg, H. B. Helle, K. D. Klem-Musatov, J. Pajchel, and B. Ursin, 2007, 3D diffraction modeling of singly scattered acoustic wavefields based on the combination of surface integral propagators and transmission operators: Geophysics, **72**, no. 5, SM19–SM34.

Baker, B. B., and E. T. Copson, 1953, The mathematical theory of Huygens' principle: Clarendon Press.

Ben-Menahem, A., and S. J. Singh, 1998, Seismic waves and sources: Dover Publications.

Brekhovskikh, L. M., 1980, Waves in layered media: Academic Press Inc.

Červený, V., 2001, Seismic ray theory: Cambridge University Press.

Červený, V., and F. Hron, 1961, Reflection coefficients for spherical waves: Studia Geophysica et Geodaetica, **5**, 122–132.

Chapman, C. H., 1994, Reflection/transmission coefficient reciprocities in anisotropic media: Geophysical Journal International, **161**, 498–501.

do Carmo, M. P., 1976, Differential geometry of curves and surfaces: Prentice Hall.

Downton, J. E., and C. Ursenbach, 2006, Linearized amplitude variation with offset (AVO) inversion with supercritical angles: Geophysics, **71**, no. 5, E49–E55.

Frazer, L. N., and M. K. Sen, 1985, Kirchhoff-Helmholtz reflection seismograms in a laterally inhomogeneous multi-layered elastic medium — I. Theory: Geophysical Journal of the Royal Astronomical Society, **80**, 121–147.

Graebner, M., 1992, Plane-wave reflection and transmission coefficients for a transversely isotropic solid: Geophysics, **57**, 1512–1519.

Hanyga, A., and H. B. Helle, 1995, Synthetic seismograms from generalized ray tracing: Geophysical Prospecting, **43**, 51–75.

Kampfmann, W., 1988, A study of diffraction-like events on DECORP 2-S by Kirchhoff theory: Journal of Geophysics, **62**, 163–174

Kennett, B. L. N., 1994, Representations of the seismic wavefield: Geophysical Journal International, **118**, 344–357.

Klem-Musatov, K. D., and A. M. Aizenberg, 1985, Seismic modelling by methods of the theory of edge waves: Journal of Geophysics, **57**, 90–105.

Klem-Musatov, K. D., A. Aizenberg, H. B. Helle, and J. Pajchel, 1993, Seismic simulation by the tip wave superposition method in complex 3D geological models: 55th Conference and Exhibition, EAGE, Extended Abstracts, P103.

———, 2004, Reflection and transmission at curvilinear interface in terms of surface integrals: Wave Motion, **39**, 77–92.

Klem-Musatov, K., A. Aizenberg, J. Pajchel, and H. B. Helle, 2008, Edge and tip diffractions: Theory and applications in seismic prospecting: SEG.

Klimeš, L., 2003, Weak-contrast reflection-transmission coefficients in a generally anisotropic background: Geophysics, **68**, 2063–2072.

Pao, Y.-H., and V. Varatharajulu, 1976, Huygens' principle, radiation conditions, and integral formulas for the scattering of elastic waves: Journal of the Acoustical Society of America, **59**, 1361–1371.

Rüger, A., 1997, P-wave reflection coefficients for transversely isotropic models with vertical and horizontal axis of symmetry: Geophysics, **62**, 713–722.

———, 2002, Reflection coefficients and azimuthal AVO analysis in anisotropic media: SEG.

Schleicher, J., M. Tygel, B. Ursin, and N. Bleistein, 2001, The Kirchhoff-Helmholtz integral for anisotropic elastic media: Wave Motion, **34**, 353–364.

Sen, M. K., and L. N. Frazer, 1991, Multifold phase space path integral synthetic seismograms: Geophysical Journal International, **104**, 479–487.

Shuey, R. T., 1985, A simplification of the Zoeppritz equations: Geophysics, **50**, 609–614.

Stovas, A., and B. Ursin, 2003, Reflection and transmission responses of layered transversely isotropic viscoelastic media: Geophysical Prospecting, **51**, 447–477.

Thomsen, L., 1993, Weak anisotropic reflections, *in* J. P. Castagna and M. M. Backus, eds., Offset dependent reflectivity — Theory and practice of AVO: SEG, 103–114.

Tsvankin, I., 1995, Seismic wavefields in layered isotropic media: Samizdat Press.

———, 2005, Seismic signatures and analysis of reflection data in anisotropic media: Elsevier.

Ursin, B., 2004, Parameter inversion and angle migration in anisotropic elastic media: Geophysics, **69**, 1125–1142.

Ursin, B., and M. Tygel, 1997, Reciprocal volume and surface scattering integrals for anisotropic elastic media: Wave Motion, **26**, 31–42.

van der Baan, M., and D. Smit, 2006, Amplitude analysis of isotropic P-wave reflections: Geophysics, **71**, no. 6, C93–C103.

Weatherburn, C. E., 1930, Differential geometry of three dimensions. vol. II: Cambridge University Press.

Wenzel, F., K.-J. Stenzel, and U. Zimmermann, 1990, Wave propagation in laterally heterogeneous layered media: Geophysical Journal International, **103**, 675–684.